IEEE Transactions on Signal Processing

Practical timing and frequency synchronization for OFDM based cooperative systems

Journal:	*Transactions on Signal Processing*
Manuscript ID:	T-SP-09091-2009
Manuscript Type:	Regular Paper
EDICS:	SPC-SYNC Acquisition, synchronization & tracking < Signal Processing for Communications, WIN-CONT Cooperative networking < Signal Processing for Wireless Networks

Practical timing and frequency synchronization for OFDM based cooperative systems

Qinfei Huang, Mounir Ghogho, Jibo Wei and Philippe Ciblat

Abstract

In this paper, we investigate the timing and carrier frequency offset (CFO) synchronization problem in decode and forward cooperative systems operating over frequency selective channels. A training sequence which consists of *one* OFDM block having a *tile* structure in the frequency domain is proposed to perform synchronization. Timing offsets are estimated using correlation-type algorithms. By inserting some null subcarriers in the proposed tile structure, we propose a computationally efficient subspace decomposition-based algorithm for CFO estimation. The issue of optimal tile length is studied both theoretically and through simulations. By judiciously designing the tile size of the pilot, the proposed algorithms are shown to have better performance, in terms of synchronization errors and bit error rate, than the time-division multiplexing-based training method and the computationally demanding SAGE algorithm.

Index Terms

Timing estimation, CFO estimation, OFDM, cooperative systems

I. Introduction

Multiple-input and multiple-output (MIMO) system is a well-known technique to increase the capacity and diversity of wireless communications. However, due to the limitations on the hardware or cost, equipping devices with multiple antennas may not be possible in some wireless networks. For this reason, a class of techniques known as cooperative communication has been introduced [1] [2]. The basic principle is to construct a virtual multiple-antenna system by sharing antennas of neighboring users in a distributed manner. The same benefits of multiple-antenna systems can be achieved in a cooperative system with proper cooperative strategies.

Different from MIMO systems, multiple nodes in these cooperative systems are not only distributed in space but also have their own oscillators, which means that there are multiple timing offsets and frequency offsets in cooperative transmission. These offsets may drastically undermine the diversity

potential of cooperative networks, see e.g. [3]. OFDM-based cooperative schemes have recently been proposed to combat timing errors (see e.g. [4] and [5].) Indeed, with a cyclic prefix (CP) insertion, OFDM is robust to limited timing errors. However, without compensation for the timing offsets, each OFDM block needs to employ an unnecessarily long CP to mitigate the interblock/multinode interference [6]. This can significantly reduce the data throughput, especially when the expected timing errors are large. Timing synchronization for all the relay nodes is therefore desirable to overcome this problem. Further, OFDM systems are very sensitive to carrier-frequency offsets (CFO). Therefore, accurate timing and frequency synchronization is key for the deployment of efficient OFDM-based cooperative systems.

To avoid the multidimensional search required by maximum-likelihood (ML) synchronization, a time division multiplexing (TDM) training based synchronization algorithm was proposed in [7]. However, although the resulting algorithms are computationally attractive, the overhead is extremely high since long guard time intervals may be required to avoid overlap of different relay node signals, especially in mobile networks where the assignment of relay nodes can be highly dynamic. A solution to obtain a good tradeoff between computational complexity and overhead is to multiplex different relay node training signals in the frequency domain. The synchronization problem then becomes similar to that in uplink OFDMA systems. Thus, synchronization algorithms for uplink OFDMA may in principle be applied to our problem. However, subband methods proposed in [8] prevents the possibility of optimally exploiting the channel diversity, and most of the other existing algorithms need to perform a complicated iterative search to estimate the timing and frequency offsets (see e.g. [9]–[12] and references therein). Further, iterative-type algorithms are sensitive to initialization. Finally and more importantly, in uplink OFDM, the received signals are processed by the base station which can afford running complex algorithms, whereas in cooperative systems, the receiver may be a mobile unit for which the computational complexity and power consumption are critical issues.

In this paper, we show that synchronization algorithms with low computational complexity and good performance can be achieved with a single OFDM training block having a *tile* structure in the frequency domain. Timing offsets are estimated using correlation-type algorithms. The CFOs are estimated using null-subcarriers inserted in the tile structure and an ESPRIT-type algorithm. By judiciously designing the size of the tile, these low-complexity algorithms are shown to have better performance, in terms of synchronization errors and bit error rate, than the computationally demanding SAGE algorithm. Unlike [13] and [14] which only consider CFO estimation for the interleaved OFDMA uplink, both timing and frequency estimation are investigated in this paper.

The rest of paper is organized as follows. In Section II, a brief introduction of the decode and forward

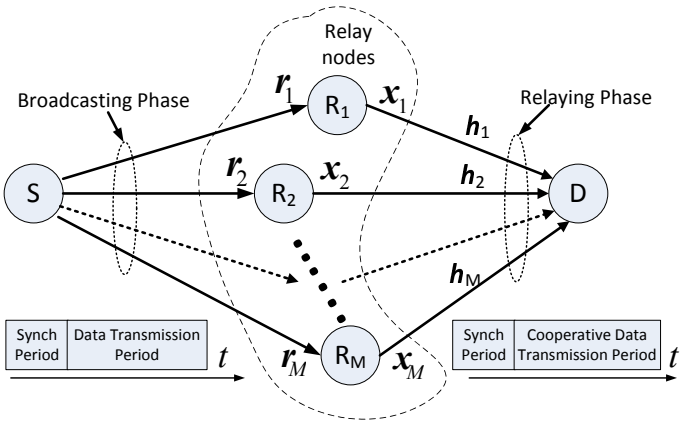

Fig. 1. Cooperative system structure

cooperative system model and tile-based training structure are presented. Synchronization algorithms are proposed in Section III. Performance analysis of the proposed algorithms is investigated in IV and verified via simulation in Section V. Finally, some conclusions are drawn in Section VI.

II. Cooperative system model

A. System description

We consider a decode and forward cooperative system with one source node, one destination node and M relay nodes as shown in Fig. 1. Training sequences are used for synchronization.

In the broadcasting phase, the source node broadcasts a training sequence followed by data blocks to the relay nodes. Each relay node operates independently. In the relaying phase, during the synchronization period, the M relay nodes transmit training sequences to the destination node. A multiple parameter estimation task is performed at the destination node. As discussed in [9], accurate timing and frequency compensation cannot be accomplished at the destination node, as the correction of one relay node's offsets would misalign the other relay nodes. To overcome this problem, the destination node may feed back the estimated offsets to the relay nodes. Then, each node can adjust its timing and frequency parameters, so that the data blocks can arrive in a synchronous manner at the destination node. Asynchronous data detection can also be carried out but its complexity may be too high for mobile nodes. It is also worth pointing out that asynchronism may provide delay diversity for flat fading channels but it may have little value in the case of frequency-selective channels. To assess the merits of our synchronization algorithm in terms of bit error rate, we consider in our simulation setup the scenario where relay nodes are synchronized

using feedback from the destination node and data transmission from the relay nodes is performed using cooperative space-time block coding.

The synchronization problem in the broadcasting phase is similar to that of a downlink OFDMA, for which single user OFDM synchronization techniques (see e.g. [15]–[17] and references therein) can be applied. Hence, we focus on the relaying phase, which is more challenging than the broadcasting phase. In principle, if the relay nodes perfectly synchronize to the source node in the broadcasting phase, the synchronization problem in the relaying phase would be simpler because there would be only one CFO to be estimated (but still multiple delay offsets). However, in practical wireless networks, synchronization is never perfect and offsets may vary over time due to node mobility and oscillator drifts.

B. Training sequence structure and receive signal model

The training sequence for each node consists of a useful part, a cyclic prefix (CP) and a cyclic postfix (PP). As in [13], the CP is composed of two parts of lengths N_{ch} and N_{dl}. The N_{ch} sample-long part of the CP is dedicated to accommodating the channel delay spreads, and the N_{dl} sample-long parts of the CP and the PP, whose length is denoted by N_{pp}, are inserted to accommodate the different propagation delays among relay nodes. It is worth pointing out that the proposed training sequences introduce a lower overhead than the TDM training sequences adopted in [7], since long guard time intervals are required by each TDM training sequence. The structure of the proposed training sequence is shown in Fig. 2.b. In this paper, we assume that the normalized CFO is less than half of the subcarrier spacing ($|\omega_i| < 0.5$) and the maximum differential propagation delay $\max\{|\tau_i - \tau_j|\}$ is smaller than $\min\{N_{dl}, N_{pp}\}$.

The useful part of the training sequence (i.e. excluding CP and PP) for each relay node consists of one OFDM block of DFT size N. The activated subcarriers are distributed among the relay nodes as follows. As depicted in Fig. 2.a, the N subcarriers are divided into P groups and each group contains Q subcarriers; P is set to be larger than the length of channel taps in order to be able to perform channel estimation. A *tile subchannel* is composed by V adjacent subchannels of each group. Parameter V will be referred to as the *tile size*. The number of subcarriers allocated to all the relay nodes in each group is set to be smaller than Q, i.e. $MV < Q$, so that null subcarriers, to be used for CFO estimation, can be inserted. The tile subchannel assigned to the ith relay node is composed of subcarriers with index set $\mathcal{M}_i = \{\eta_{i,v,p} = v+pQ+(i-1)V, v = 0, ..., V-1; p = 0, ..., P-1\}$. Letting $\boldsymbol{X}_i = [X_i(0) \cdots X_i(N-1)]^T$ and $\boldsymbol{x}_i = [x_i(0) \cdots x_i(N-1)]^T$ respectively denote the frequency and time domain training sequences

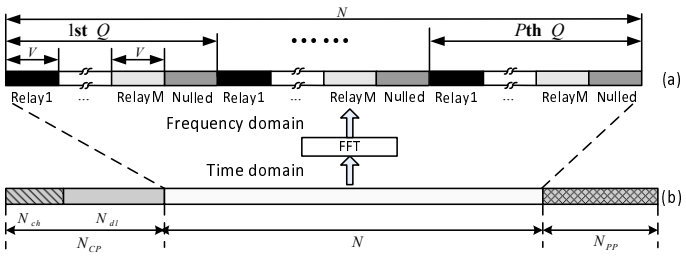

Fig. 2. Training structure illustration

of the ith user, we have that

$$x_i(n) = \frac{1}{\sqrt{N}} \sum_{v=0}^{V-1} \sum_{p=0}^{P-1} X_i(\eta_{i,v,p}) e^{j2\pi\eta_{i,v,p}n/N}, \quad n = 0, \cdots, N-1 \tag{1}$$

After adding the CP, the transmitted training sequences can be expressed as

$$x_i(n) = \begin{cases} x_i(N+n) & n = -1, \cdots, -N_{cp} \\ x_i(n) & n = 0, \cdots, N-1 \\ x_i(n-N) & n = N, \cdots, N+N_{pp-1} \end{cases}$$

Removing the CP and collecting the first N samples, the received version of the training signal at the destination node can be written as

$$r(n) = \sum_{i=1}^{M} e^{j2\pi\omega_i n/N} \sum_{l=0}^{L-1} h_i(l) x_i(n-l-\tau_i) + v(n), \quad n = 0, \cdots, N-1 \tag{2}$$

where $\boldsymbol{h}_i = [h_i(0) \cdots h_i(L-1)]^T$, τ_i and ω_i are respectively the channel impulse response (CIR), the integer part of the normalized (to the sampling period) delay and the normalized (to the inverse of the symbol period) CFO associated with the ith relay node, and $v(n)$ is an AWGN with variance σ_v^2. Since OFDM modulation is used, the fractional part of the propagation delay and initial phase are not explicitly included in the above signal model because they can be incorporated into the channel frequency response.

Letting $\boldsymbol{r} = [r(0) \cdots r(N-1)]^T$, $\boldsymbol{\Gamma}(\omega_i) = \text{diag}\{1, e^{j2\pi\omega_i/N}, \cdots, e^{j2\pi\omega_i(N-1)/N}\}$; $[\mathbf{X}_{\tau_i}]_{m,n} = x_i(m-n-\tau_i)$, where $m = 0, \cdots, N-1$ and $n = 0, \cdots, L-1$, and $\boldsymbol{v} = [v(0) \cdots v(N-1)]^T$, vector $\boldsymbol{r}$ can, using Eq (2), be expressed as

$$\boldsymbol{r} = \mathbf{A}_{\boldsymbol{\omega},\boldsymbol{\tau}} \boldsymbol{h} + \boldsymbol{v} \tag{3}$$

where $\mathbf{A}_{\boldsymbol{\omega},\boldsymbol{\tau}} = [\boldsymbol{\Gamma}(\omega_1)\mathbf{X}_{\tau_1}, \cdots, \boldsymbol{\Gamma}(\omega_M)\mathbf{X}_{\tau_M}]$; $\boldsymbol{h} = [\boldsymbol{h}_1^T \cdots \boldsymbol{h}_M^T]^T$; $\boldsymbol{\omega} = [\omega_1, \cdots, \omega_M]^T$; $\boldsymbol{\tau} = [\tau_1, \cdots, \tau_M]^T$.

The joint ML estimators of the timing and CFO parameters can be readily expressed as

$$(\hat{\boldsymbol{\tau}}, \hat{\boldsymbol{\omega}}) = \arg\max_{\boldsymbol{\tau},\boldsymbol{\omega}} \left\{ \boldsymbol{r}^H \mathbf{A}_{\boldsymbol{\omega},\boldsymbol{\tau}} \left(\mathbf{A}_{\boldsymbol{\omega},\boldsymbol{\tau}}^H \mathbf{A}_{\boldsymbol{\omega},\boldsymbol{\tau}} \right)^{-1} \mathbf{A}_{\boldsymbol{\omega},\boldsymbol{\tau}}^H \boldsymbol{r} \right\}. \tag{4}$$

The maximization in (4) requires a search over the $2M$ dimensional domain spanned by $(\boldsymbol{\omega}, \boldsymbol{\tau})$, which may not be tractable in practice. Unlike [7] which uses a TDM training sequence to avoid the multidimensional search, we adopt a frequency-domain multiplexing for our training design in order to obtain low overhead.

III. Timing and frequency offsets estimation

A. Timing offsets estimation algorithm

In this subsection, we present a Weighted Slide Cross-correlation Timing Estimator (WSCTE), which can estimate each relay node timing parameter readily and accurately by exploring the cross correlation between the received signal and each relay node's training sequence.

Using the above training structure, the received signal can be re-expressed as

$$r(n) = \sum_{i=1}^{M} r^{(i)}(n) + v(n), \;\; n = 0, \cdots, N-1 \tag{5}$$

where $r^{(i)}(n) = \sum_{v=0}^{V-1} r^{(i,v)}(n)$ and

$$r^{(i,v)}(n) = \frac{1}{\sqrt{N}} e^{j\phi_i} e^{j\theta_{i,v}(n-\tau_i)} \sum_{p=0}^{P-1} X_i(\eta_{i,v,p}) H_i(\eta_{i,v,p}) e^{j2\pi p(n-\tau_i)/P} \tag{6}$$

where $\phi_i = 2\pi\omega_i\tau_i/N$; $\theta_{i,v} = 2\pi(\omega_i + v + (i-1)V)/N$ is a CFO-related parameter, and $H_i(k)$ is the channel frequency response at the kth subcarriers of the ith relay node.

Let $Z_{i,k}(\tilde{\tau}, \omega_i) \triangleq \sum_{n=0}^{N-1} r^{(i)}(n+\tilde{\tau}) x_k^*(n)$. Using eq. (6), we get

$$Z_{i,k}(\tilde{\tau}, \omega_i) = \begin{cases} 0 & i \neq k, \;\; \omega_i = 0; \\ Q \sum_{v_1=v_2=0}^{V-1} Y_{i,i}(\tilde{\tau}, 0) & i = k, \;\; \omega_i = 0; \\ \sum_{v_1=0}^{V-1} \sum_{v_2=0}^{V-1} \epsilon_{i,k}(\omega_i) Y_{i,k}(\tilde{\tau}, \omega_i) & \omega_i \neq 0 \end{cases} \tag{7}$$

where $\epsilon_{i,k}(\omega_i) \triangleq \frac{1-e^{j2\pi\omega_i}}{1-e^{j2\pi(\rho_{i,v_1} - \rho_{k,v_2} + \omega_i)/Q}}$, $\rho_{i,v} = v + (i-1)V$ and

$$Y_{i,k}(\tilde{\tau}, \omega_i) \triangleq \frac{1}{N} e^{j\phi_i} \sum_{n=0}^{P-1} e^{-j\theta_{i,v_1}(\tau_i - \tilde{\tau})} e^{j2\pi(\rho_{i,v_1} - \rho_{k,v_2} + \omega_i)n/N} g_{i,v_1}(n - \tau_i + \tilde{\tau}) f_{k,v_2}^*(n)$$

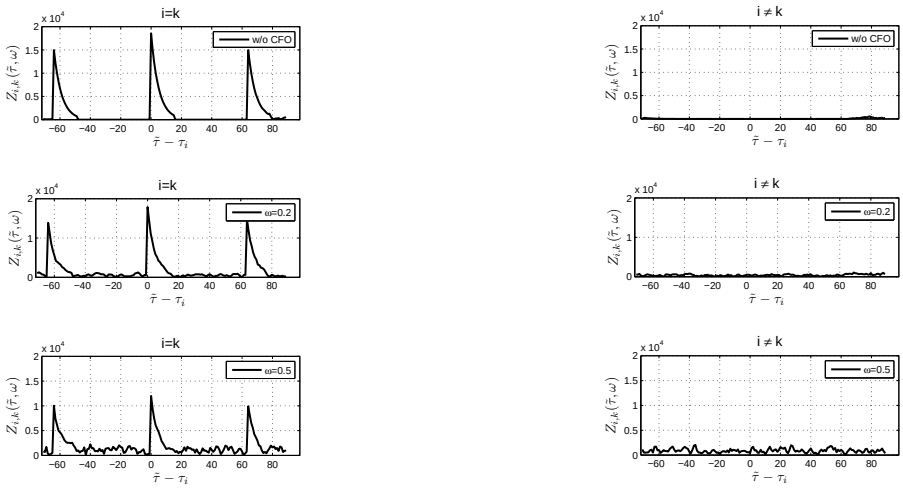

Fig. 3. $Z_{i,k}(\tilde{\tau},\omega_i)$ versus $\tilde{\tau}-\tau_i$ for different values of ω_i; $N=512$, $L=16$, $V=3$, $Q=8$

where $f_{i,v}(n) \triangleq \sum_{p=0}^{P-1} X_i(\eta_{i,v,p}) e^{j2\pi np/P}$, $g_{i,v}(n) \triangleq \sum_{p=0}^{P-1} X_i(\eta_{i,v,p}) H_i(\eta_{i,v,p}) e^{j2\pi np/P}$, and $*$ denotes the complex conjugate operator.

It can be deduced from the first and second terms in the RHS of eq. (7) that the received signal has good correlation properties. However, in the presence of CFO, the above results do not hold anymore. Nevertheless, since the normalized CFO is assumed to be less than half of the subcarriers spacing, it can be verified that the effect of the CFO can be neglected as shown in Fig. 3. Exploiting multipath diversity, the proposed WSCTE algorithm is given by

$$\hat{\tau}_i = \arg\max_{\tilde{\tau}_i} J(\tilde{\tau}_i) \tag{8}$$

where

$$J(\tilde{\tau}_i) = \sum_{l=0}^{L-1} \alpha_l \left| \sum_{n=0}^{N-1} r(n+\tau_i+l) x_i^*(n) \right|^2 \tag{9}$$

and $\boldsymbol{\alpha} = [\alpha_0 \ \cdots \ \alpha_{L-1}]^T$ are weighting coefficients, whose optimal design will be addressed later.

B. CFOs estimation algorithm

Once the timing offset estimation is carried out, we collect samples of the received signal as follows. The starting point of this set of samples is determined by the estimated timing parameter of the relay node whose signal arrives first at the destination. We assume that the timing offset estimation error of the first arrival signal is within the interblock-interference-free zone, $[-N_{CP}+\Delta\tau_{1M}+N_{ch},\ N_{PP}-1]$, as

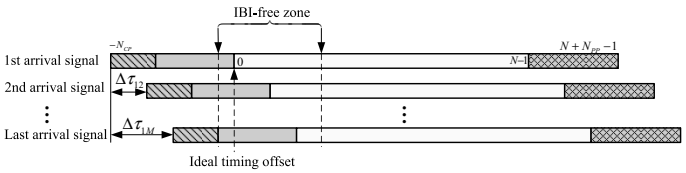

Fig. 4. Illustration of interblock-interference-free zone for timing offset estimation error

shown in Fig. 4, where $\Delta\tau_{1M}$ denotes the timing offset between the first and last arriving signals, so that the receive signal at the destination node still has a per-component repetitive structure. Let $\{\tilde{r}(n)\}_{n=0}^{N-1}$ denote the collected N samples after timing offset estimation. From eq. (5), we get

$$\tilde{r}(n+\mu P) = \sum_{i=1}^{M}\sum_{v=0}^{V-1} e^{j\theta_{i,v}\mu P}\tilde{r}^{(i,v)}(n) + \upsilon(n+\mu P) \qquad (10)$$
$$n = 0, \cdots, P-1,\ \mu = 0, \cdots, Q-1$$

We then arrange the N samples into a $Q \times P$ matrix

$$\mathbf{R} = \begin{bmatrix} \tilde{r}(0) & \cdots & \tilde{r}(P-1) \\ \tilde{r}(P) & \cdots & \tilde{r}(2P-1) \\ \vdots & \ddots & \vdots \\ \tilde{r}((Q-1)P) & \cdots & \tilde{r}(N-1) \end{bmatrix}_{Q\times P} \qquad (11)$$

Letting $\boldsymbol{R}_p$ denote the pth column of matrix $\mathbf{R}$, we have that

$$\boldsymbol{R}_p = \mathbf{G}\tilde{\boldsymbol{r}}_p + \boldsymbol{\upsilon}_p,\ l = 0, \cdots, P-1 \qquad (12)$$

where $\tilde{\boldsymbol{r}}_p = \left[\tilde{r}^{(1,0)}(p)\ \tilde{r}^{(1,1)}(p)\ \cdots\ \tilde{r}^{(M,V-1)}(p)\right]^T$ and $\mathbf{G}$ is a $(Q \times MV)$ matrix given by

$$\mathbf{G} = \begin{bmatrix} 1 & 1 & \cdots & 1 \\ e^{j\theta_{1,0}P} & e^{j\theta_{1,1}P} & \cdots & e^{j\theta_{M,V-1}P} \\ \vdots & \vdots & \ddots & \vdots \\ e^{j\theta_{1,0}(Q-1)P} & e^{j\theta_{1,1}(Q-1)P} & \cdots & e^{j\theta_{M,V-1}(Q-1)P} \end{bmatrix}$$

The main idea behind the proposed low-complexity CFO estimation algorithm is to first estimate the $\theta_{i,v}$'s, which are distinct from each other since the ω_i's are assumed to be less than 0.5 in absolute value, and then appropriately combine estimates of the $\theta_{i,v}$'s to obtain the CFO estimates. This approach allows us to estimate the multiple CFOs using *one* OFDM symbol. Indeed, the $\theta_{i,v}$'s in eq. (10) cause phase shifts to identical P-sample long segments. Hence, our approach can in a way be seen as an extension of the repetitive-slot CFO estimation approach (see e.g. [18], [19]) to the case of multiple CFO estimation.

Once we express the received samples as in eq. (10), CFO estimation can be carried out using a signal subspace decomposition approach. The dimension of the null subspace is dictated by the number of null subcarriers, which is equal to $Q - MV$. CFO estimation for single user OFDM using null subcarriers was studied in e.g. [20] and references therein. Thus, to estimate the multiple CFOs, subspace based methods (MUSIC and ESPRIT) are known to provide low complexity algorithms, compared to the ML method. Here we adapt one of the modified versions of ESPRIT, namely forward-backward smoothing ESPRIT (FBS-ESPRIT) [21] to our CFO estimation problem.

The multiple CFOs are estimated using the following steps:

Step 1) Arrange the received signal $\tilde{\boldsymbol{r}}$ into matrix $\mathbf{R}$.

Step 2) The covariance matrix $\boldsymbol{\Omega} = \mathrm{E}\left\{\boldsymbol{R}_p \boldsymbol{R}_p^H\right\}$ of $\boldsymbol{R}_p$ is estimated by using the forward-backward smoothing principle as

$$\widehat{\boldsymbol{\Omega}} = \frac{1}{2}\left(\tilde{\boldsymbol{\Omega}} + \mathbf{J}\tilde{\boldsymbol{\Omega}}^T\mathbf{J}\right)$$

where $\tilde{\boldsymbol{\Omega}} = \frac{1}{P}\mathbf{R}\mathbf{R}^H$ and $\mathbf{J}$ is the exchange matrix with 1's on the anti-diagonal and 0's elsewhere.

Step 3) Compute singular value decomposition (SVD) of $\widehat{\boldsymbol{\Omega}}$, and arrange the eigenvectors of $\widehat{\boldsymbol{\Omega}}$ that are associated to the MV largest eigenvalues $\lambda_1 \geq \lambda_2 \geq \cdots \geq \lambda_{MV}$ into a $Q \times MV$ matrix $\mathbf{U}_s$. Let $\mathbf{U}_{s1}$ denote the first $(Q-1)$ rows of $\mathbf{U}_s$ and $\mathbf{U}_{s2}$ denote the last $(Q-1)$ rows of $\mathbf{U}_s$. The $\theta_{i,v}$'s are estimated as

$$\hat{\theta}_{i,v} = \frac{1}{P}\arg(\beta_k), \qquad k = v + (i-1)V \tag{13}$$

where $\{\beta_k\}_{k=0}^{MV-1}$ are the eigenvalues of

$$\boldsymbol{\Xi} = \left(\mathbf{U}_{s1}^H\mathbf{U}_{s1}\right)^{-1}\mathbf{U}_{s1}^H\mathbf{U}_{s2}$$

.

Step 4) After getting the $\hat{\theta}_{i,v}$'s, we adopt, for simplicity, equal gain combining (EGC) to compute the CFO estimate for each relay node. Thus, the proposed EGC-FBS-ESPRIT-based CFO estimator, which will be referred to as EFCE, is given by

$$\hat{\omega}_i = \frac{1}{V}\sum_{v=0}^{V-1}\left(\frac{N\hat{\theta}_{i,v}}{2\pi} - v\right) - i + 1, \;\; i = 1, \cdots, M \tag{14}$$

Another subspace-based methods (Spectral MUSIC and total least square ESPRIT) has been applied to the interleaved OFDMA uplink system in [13] and [14]. However, it is worth pointing out that the interleaved subcarriers allocation is a special case ($V = 1$) of the proposed pilot structure. We will see later that $V = 1$ is not a good choice.

IV. Performance analysis

Since timing and frequency offsets are respectively discrete and continuous parameters, it is complicated to analyze the timing and frequency offsets estimation performance jointly. Therefore, we investigate the performance of the proposed estimation algorithms, WSCTE and EFCE, separately.

A. WSCTE weights selection

From eq. (8), the optimal weights can be obtained by optimizing the following equation

$$\boldsymbol{\alpha}^o = \arg\max_{\boldsymbol{\alpha}} \Pr(J(\tilde{\tau}_i = \tau_i) > J(\tilde{\tau}_i \neq \tau_i)|\boldsymbol{\alpha}) \tag{15}$$

under the constraint $\sum_{l=0}^{L-1} \alpha_l = 1$, where $\Pr(a|b)$ denotes the conditional probability. However, since the $J(\tilde{\tau}_i)$'s are dependent Gamma distributed variables, it is cumbersome to derive a close-form expression for the conditional probability. Hence, a numerical suboptimal solution is desired.

We consider a class of weights which satisfy $\alpha_l = C_\gamma e^{-\gamma l}$, where $\gamma = (-\infty, +\infty)$ and C_γ is a scalar factor that ensures that the sum of all weights is normalized to unity. It is worth pointing out that $\boldsymbol{\alpha}$ approximates $[1, 0, \cdots, 0]^T$ for sufficiently large positive γ, which is the weight vector used in [22], [23]. We will show that the performance of WSCTE can be much improved by judiciously selecting the weights.

To simplify the performance analysis of timing estimation, we consider the case without CFOs in this and the following subsections. It is worth pointing out that the results hold true even in the presence of CFO values considered in this paper. Fig. 5 shows the standard deviation of WSCTE versus various γ. Both the exponential power delay profile, i.e. ($\mathrm{E}\left\{|h_i(l)|^2\right\}_{l=0}^{L-1} = C\exp(-0.2l)$ where C is a scalar factor that ensures that the total energy of the channel taps is normalized to unity) and the uniform power delay ($\mathrm{E}\left\{|h_i(l)|^2\right\}_{l=0}^{L-1} = 1/L$) profile have been tested. Fig. 5 clearly shows that $\gamma = 0$ gives the best estimation performance among all examined values of γs. Hence, $\boldsymbol{\alpha} = [1, \cdots, 1]^T/L$ is adopted in this paper.

B. Tile size selection for WSCTE

We define the optimal tile size for WSCTE as the value of V that maximizes the probability of exact determination of the delays, i.e.

$$V^o = \arg\max_{V} \Pr(J(\tilde{\tau}_i = \tau_i) > J(\tilde{\tau}_i \neq \tau_i)|V) \tag{16}$$

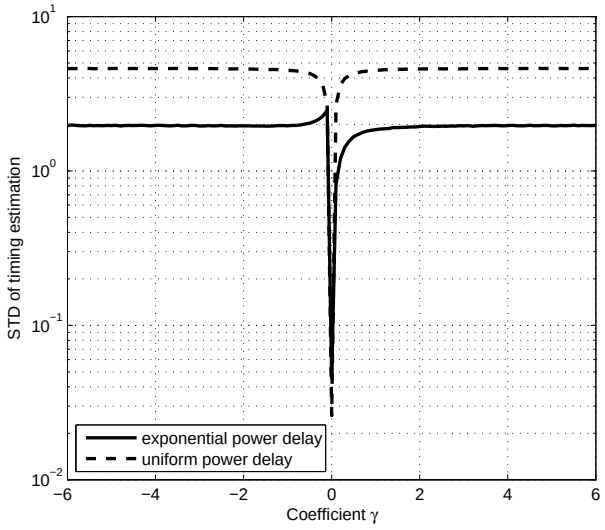

Fig. 5. γ Versus standard deviation of timing estimation, $N = 512$, $L = 16$, $M = 2$, $V = 3$, $Q = 8$, SNR=20dB

As for eq. (15), it is analytically untractable to solve the above optimization problem. As shown in Fig. 3, we can notice that a wrong estimate of τ_i will most likely be in the set $\{\tau_i \pm 1, \tau_i \pm P\}$. Thus, we simplify the above optimization problem as follows

$$V^o = \arg\min_{V} \sum_{n=1}^{4} \mathrm{Pr}_n(V) \tag{17}$$

where $\mathrm{Pr}_1(V) = \mathrm{Pr}(J(\tilde{\tau}_i = \tau_i) < J(\tilde{\tau}_i = \tau_i + 1)|V)$; $\mathrm{Pr}_2(V) = \mathrm{Pr}(J(\tilde{\tau}_i = \tau_i) < J(\tilde{\tau}_i = \tau_i - 1)|V)$; $\mathrm{Pr}_3(V) = \mathrm{Pr}(J(\tilde{\tau}_i = \tau_i) < J(\tilde{\tau}_i = \tau_i + P)|V)$ and $\mathrm{Pr}_4(V) = \mathrm{Pr}(J(\tilde{\tau}_i = \tau_i) < J(\tilde{\tau}_i = \tau_i - P)|V)$.

Without CFOs, eq. (9) can be rewritten as

$$J(\tilde{\tau}_i) = \sum_{l=0}^{L-1} \alpha_l \left| Z_{i,i}(\tilde{\tau}_i + l, 0) + d_i(\tilde{\tau}_i + l) \right|^2 \tag{18}$$

where $d_i(\tilde{\tau}_i + l) = \sum_{n=0}^{N-1} \upsilon(n + \tilde{\tau}_i + l) x_i^*(n)$. We assume that the training sequences of different relay nodes are uncorrelated and power constrained, i.e. $\sum_{n=0}^{N-1} |X_i(n)|^2 = \sigma_{ts}^2$. Using $\boldsymbol{\alpha} = [1, \cdots, 1]^T / L$ as weights and after some tedious manipulation (see Appendix A), for high SNR, we obtain

$$\begin{aligned} \mathrm{E}\left\{J(\tau_i) - J(\tau_i + 1)\right\} &= \frac{\sigma_{ts}^4}{L} \mathrm{E}\left\{|h_i(0)|^2\right\} \\ \mathrm{Var}\{J(\tau_i) - J(\tau_i + 1)\} &= \frac{\sigma_{ts}^8}{L^2} \mathrm{E}\left\{|h_i(0)|^2\right\}^2 \end{aligned} \tag{19}$$

$$\begin{aligned} \mathrm{E}\left\{J(\tau_i) - J(\tau_i - 1)\right\} &= \frac{\sigma_{ts}^4}{L}\mathrm{E}\left\{|h_i(L-1)|^2\right\} \\ \mathrm{Var}\{J(\tau_i) - J(\tau_i - 1)\} &= \frac{\sigma_{ts}^8}{L^2}\mathrm{E}\left\{|h_i(L-1)|^2\right\}^2 \end{aligned} \tag{20}$$

$$\begin{aligned} \mathrm{E}\left\{J(\tau_i) - J(\tau_i \pm P)\right\} &= \frac{\sigma_{ts}^4}{LV^2}(V^2 - \xi(\pm P)) \\ \mathrm{Var}\{J(\tau_i) - J(\tau_i \pm P)\} &= \frac{\sigma_{ts}^8}{L^2V^4}(V^2 - \xi(\pm P))^2 \\ &\quad \sum_{l=0}^{L-1}\mathrm{E}\left\{|h_i(l)|^2\right\}^2 \end{aligned} \tag{21}$$

where $\xi(\pm P)$ is defined in eq. (35) in the appendix. The following remarks are in order.

1) $\mathrm{Pr}_1(V)$ and $\mathrm{Pr}_2(V)$ are independent of V.
2) For $V = 1$, we have that $\mathrm{E}\left\{J(\tau_i) - J(\tau_i \pm P)\right\} = 0$ and $\mathrm{Var}\{J(\tau_i) - J(\tau_i \pm P)\} = 0$, which means that $V = 1$ causes ambiguities in timing estimation. These ambiguities vanish for larger values of V.
3) Since the coefficient of variation of $J(\tau_i) - J(\tau_i \pm P)$, defined as $\sqrt{\mathrm{Var}\{J(\tau_i) - J(\tau_i \pm P)\}}/\mathrm{E}\left\{J(\tau_i) - J(\tau_i \pm P)\right\}$, is independent of V for $V > 1$, the dispersion of $J(\tau_i) - J(\tau_i \pm P)$ is independent of V and larger $\mathrm{E}\left\{J(\tau_i) - J(\tau_i \pm P)\right\}$ will give smaller $\mathrm{Pr}_3(V)$ and $\mathrm{Pr}_4(V)$.
4) The optimal V can be approximated by

$$V^o \approx \arg\max_V \{\sum_{i=1}^{4} \chi_i\} \tag{22}$$

where $\chi_1 = \mathrm{E}\left\{J(\tau_i) - J(\tau_i + 1)\right\}/\mathrm{E}\left\{J(\tau_i)\right\}$, $\chi_2 = \mathrm{E}\{J(\tau_i) - J(\tau_i - 1)\}/\mathrm{E}\left\{J(\tau_i)\right\}$, $\chi_3 = \mathrm{E}\{J(\tau_i) - J(\tau_i + P)\}/\mathrm{E}\left\{J(\tau_i)\right\}$ and $\chi_4 = \mathrm{E}\{J(\tau_i) - J(\tau_i - P)\}/\mathrm{E}\left\{J(\tau_i)\right\}$. We readily obtain

$$\begin{aligned} \chi_1 = \mathrm{E}\left\{|h_i(0)|^2\right\};\ \chi_2 = \mathrm{E}\left\{|h_i(L-1)|^2\right\} \\ \chi_3 = \chi_4 = 1 - \left(\frac{\sin(\pi V n/Q)}{V\sin(\pi n/Q)}\right)^2 \end{aligned} \tag{23}$$

Since χ_1 and χ_2 are independent of V, the optimization problem (22) can be further simplified as

$$V^o \approx \arg\max_V \chi_3 \tag{24}$$

Fig. 6 shows a numerical example of the impact of tile size on $\{\chi_n\}_{n=1}^3$ when $N = 512$, $L = 16$ and $M = 2$ and $Q = 2^{\lfloor \log_2 MV \rfloor + 1}$. The exponential power delay profile introduced previously was considered. For this numerical example, it can be deduced that:

1) for the evaluated tile sizes, $V = 7$ will provide the best timing estimation performance;

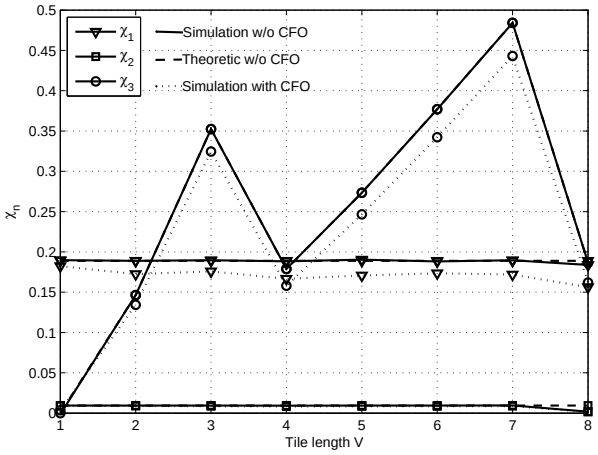

Fig. 6. χ_n Versus tile size V, $N = 512$, $L = 16$, $M = 2$, $Q = 2^{\lfloor \log_2 MV \rfloor + 1}$, SNR=20dB, CFO case $\omega_1 = \omega_2 = 0.5$

2) since the timing offset error is dominated by the larger $\Pr_i$, the estimation performance versus tile size V will encounter a floor due to the fact that χ_1 and χ_2 remain constant when varying V; further, $V = 3$ will yield performance close to those of $V = 5, 6, 7$;
3) the results hold true in the presence of CFOs.

The above results will be verified through simulations in Section V. For different signal parameters, the values for the best tile sizes may differ from those given above. These can be accurately predicted by eq. (24).

C. CFO estimation performance analysis

To analyze the performance of the proposed CFO estimator, we assume perfect timing, and use the Cramér-Rao bound associated with the estimation of the $\theta_{i,v}$'s based on the signal model in eq. (10), where the $\tilde{r}^{i,v}(n)$'s are treated as deterministic unknowns,[1] and then deduce bounds on the estimation of the ω_i's using the relationships in eq. (14). The obtained bound will be referred to the subspace decomposition based CRB (SD-CRB) since eq. (10) allows CFO estimation using subspace-based methods.

[1]Such an approach was adopted in [19] for the case of single CFO estimation

The SD-CRB of $\boldsymbol{\theta}$ is obtained along the same lines as in [24] and is found to be

$$\text{SD-CRB}_{(V,P)}(\boldsymbol{\theta}) = \frac{\sigma_v^2}{2}\left\{\sum_{p=0}^{P-1}\text{Re}\left\{\mathbf{D}_p^H\mathbf{T}^H \left(\mathbf{I}-\mathbf{G}\left(\mathbf{G}^H\mathbf{G}\right)^{-1}\mathbf{G}^H\right)\mathbf{T}\mathbf{D}_p\right\}\right\}^{-1} \tag{25}$$

where $\boldsymbol{\theta} = [\boldsymbol{\theta}_1^T, \cdots, \boldsymbol{\theta}_M^T]^T$, $\boldsymbol{\theta}_i = [\theta_{i,0}, \cdots, \theta_{i,V-1}]^T$, $\mathbf{T} = [\frac{\partial(\boldsymbol{G}_0)}{\partial\theta_{1,0}}, \frac{\partial(\boldsymbol{G}_1)}{\partial\theta_{1,1}}, \cdots, \frac{\partial(\boldsymbol{G}_{MV})}{\partial\theta_{M,V-1}}]$, $\boldsymbol{G}_l$ is the lth column of matrix $\mathbf{G}$; and $\mathbf{D}_p = \text{diag}\{\tilde{\boldsymbol{r}}_p\}$. Recall eq. (14), we have

$$\omega_i = \frac{N}{2\pi V}\boldsymbol{\zeta}^T\boldsymbol{\theta}_i - c_i$$

where $\boldsymbol{\zeta} = [1, \cdots, 1]^T$ and $c_i = i - 1 + \frac{1}{V}\sum_{v=0}^{V-1} v$. The SD-CRB for $\hat{\omega}_i$ can be expressed as

$$\text{SD-CRB}(\omega_i) = \left(\frac{N}{2\pi V}\right)^2 \boldsymbol{\zeta}^T\text{SD-CRB}_{(V,P)}(\boldsymbol{\theta}_i)\boldsymbol{\zeta} \tag{26}$$

where $\text{SD-CRB}_{(V,P)}(\boldsymbol{\theta}_i)$ is a sub-matrix of $\text{SD-CRB}_{(V,P)}(\boldsymbol{\theta})$. We can see later that the performance of the EFCE method with the proposed WSCTE estimator could approach the SD-CRB by selecting the title size V properly. It can be shown that $V = 1$ is optimal for CFO estimation in the absence of timing offset. When timing is required to be estimated, $V = 1$ will be shown in the simulation section to yield poor CFO estimation performance.

V. Simulation results

A. Simulation setup

Consider a cooperative system with two relay nodes, i.e. $M = 2$. The total number of subcarriers of each OFDM block is $N = 512$. The training sequences of the relay nodes are uncorrelated and have the same power σ_{ts}^2. The CP and PP of the training sequences are selected to have lengths equal to 64 and 48, respectively. In order to satisfy the condition that $\max\{|\tau_i - \tau_j|\} < \min\{N_{dl}, N_{pp}\}$, we assume that the signal of relay node R_1 arrives at the destination node first in our simulation setup, and the differential propagation delay $\tau_2 - \tau_1$ is uniformly distributed within the interval $[0, 48]$. The tile subchannels allocated to the two relay nodes during the training period are distinct. To make sure Q is larger than MV, we select $Q = 2^{\lfloor \log_2 MV \rfloor + 1}$, where $\lfloor a \rfloor$ rounds a to the nearest integer smaller than or equal to a. Hence, the number of null subcarriers is 256, 256, 128, 256, 192, 128, 64, and 256 when V increases from 1 to 8, respectively.

In the simulation, we assume that the CIR length is $L = 16$, and the channel taps $h_i(l)$ are uncorrelated zero-mean Gaussian random variables with exponential power delay profile $\text{E}\left\{|h_i(l)|^2\right\}_{l=0}^{L-1} =$

$C\exp(-0.2l)$, where C is a scalar factor that ensures that the total energy of the channel taps is normalized to unity. Correspondingly, the SNR of each relay node is equal to $\sigma_{ts}^2/(N\sigma_v^2)$. The channels for different nodes are assumed uncorrelated.

To quantify the degradation of the BER due to the residual timing and CFO, which are equal to the difference between the offset estimates fed back by the destination node and the actual offsets, information-bearing blocks are transmitted using a cooperative Alamouti space-time encoding and maximum likelihood detection assuming a perfect channel state information is performed.

B. Simulation results

In this section, we compare the estimation performance of the proposed algorithms and the conventional SAGE algorithm in [11] and TDM based S&C algorithm [15]. The SAGE estimation results shown are obtained at the 5th iteration and CIR are assumed to be known perfectly in each iteration. The length of TDM based training sequences is set to N/M to make a fair comparison. We also assume that there is no collision for TDM based synchronization.

Fig. 7 and Fig. 8 show the timing estimation performance of the proposed WSCTE with different tile sizes. The estimation performance is measured in terms of averaged (over the channel and relay nodes) standard deviation (STD) of the timing errors. As predicted in the previous section, we see that the WSCTE with tile size $V = 3, 5, 6, 7$ outperforms other selections significantly. Moreover, we can find that improvement shrinks for large tile sizes. The tile size $V = 3$ seems to provide sufficient accuracy. It can also be seen that WSCTE performance is dominated by multinode interference since it is not very sensitive to SNR. It can also be seen that the proposed WSCTE with tile size $V = 3$ outperforms TDM based and SAGE algorithms significantly.

Figures 9-11 compare the CFO estimation performance of EFCE with different tile sizes. The performance is measured in terms of averaged (over the channel and relay nodes) MSE. We set the frequency offsets to $\omega_1 = 0.35$ and $\omega_2 = 0.25$. It can be seen that EFCE with tile size $V = 1$ provides the best performance at low SNR. However, it exhibits an error floor at intermediate and high SNRs due to the residual timing errors. As shown in Fig. 9 and Fig. 10, we also notice that the performance of EFCE with the tile size that provides the best timing estimate, i.e. $V = 3$ in the above figures, achieves the SD-CRB. Moreover, we can see from Fig. 11 that the proposed EFCE, with tile size $V = 3$, outperforms the TDM based and SAGE algorithms.

The BER performance of an uncoded QPSK system is shown in Fig. 12. A cooperative Alamouti space-time encoding scheme is adopted and the channels, which take into account timing errors, are

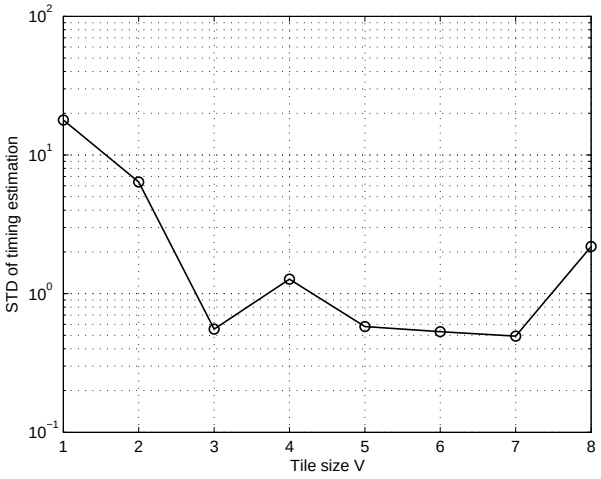

Fig. 7. WSCTE estimation performance versus tile size V, SNR=20dB

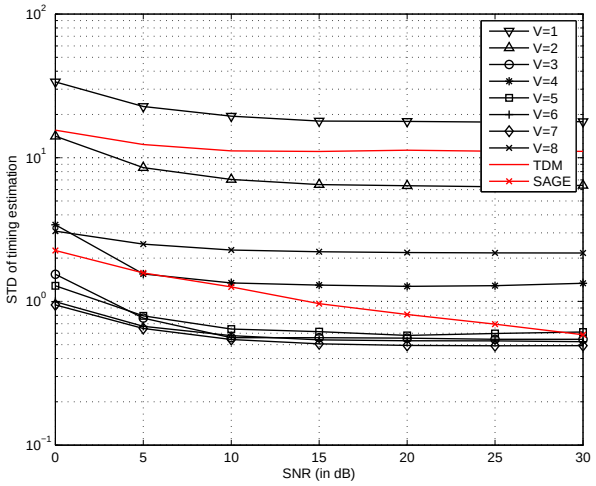

Fig. 8. Timing estimation performance versus SNR

assumed to be known. The length of the CP for the data blocks is set to 20. As expected, SAGE and TDM-based algorithms are outperformed by the proposed algorithms. It can be seen that tile size $V = 3$ outperforms the other evaluated tile sizes at intermediate and high SNRs, and the corresponding BER performance is close to the ideal case scenario (no synchronization errors).

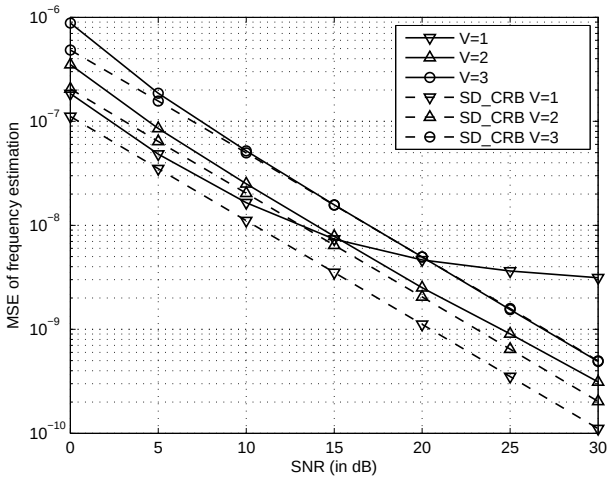

Fig. 9. EFCE estimation performance versus SNR

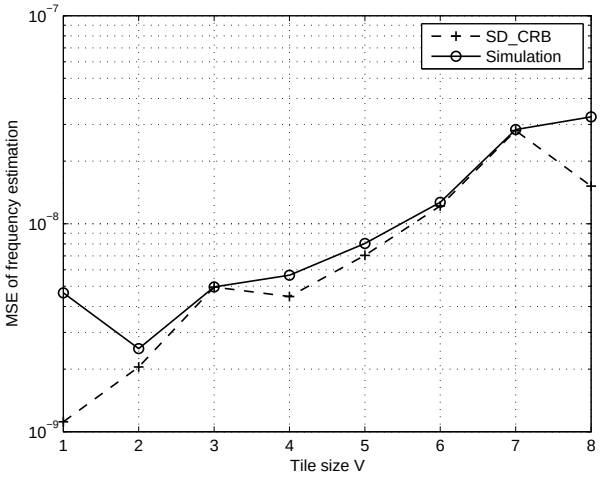

Fig. 10. EFCE estimation performance versus tile size V, SNR=20dB

C. Optimal tile size selection for BER

As shown in WSCTE performance evaluation, larger tile sizes will provide better timing estimation performance. However, EFCE performance will decrease with increasing tile size. Due to the estimation floor of WSCTE, as discussed previously, we can conclude that a good BER performance is achieved by the smallest tile size with close-best timing performance. The optimal tile size can be predicted as shown in Section IV.B.

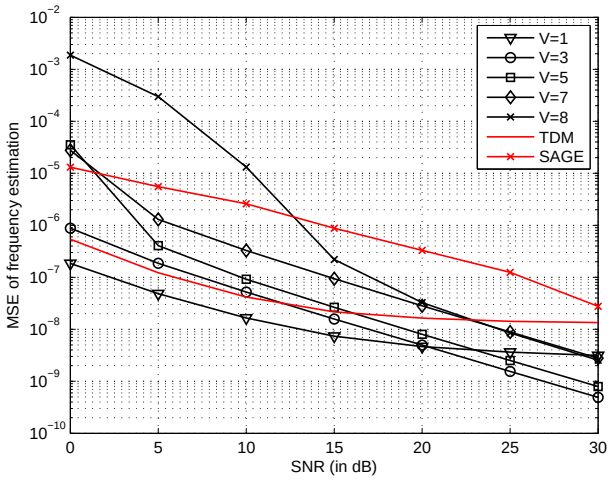

Fig. 11. CFO estimation performance versus SNR

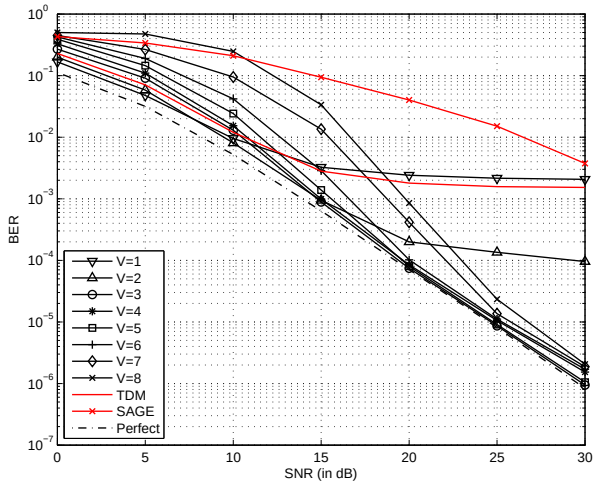

Fig. 12. BER performance versus SNR for uncoded QPSK

D. Computational Complexity

We briefly compare the complexities of the proposed synchronization algorithms and SAGE. Considering the number of complex multiplications as a complexity metric, the inversion of an $n \times n$ matrix requires $\mathcal{O}(n^3)$ operations, the SVD of $n \times n$ matrix requires $\mathcal{O}(n^3)$ operations, and the product of an $m \times r$ matrix with an $r \times n$ matrix requires $\mathcal{O}(mrn)$ operations.

Assume that the WSCTE and SAGE algorithms need to search over the same time interval of length, say

K_t, for timing estimation. The complexity of WSCTE is $\mathcal{O}(K_t MN)$, and SAGE needs $\mathcal{O}(K_t MNLK_{it})$ operations, where K_{it} denotes the number of iterations. Regarding CFO estimation, SAGE takes $\mathcal{O}(MNLK_{it}K_f)$ operations, where $K_f > 10^3$ denotes the number of evaluated CFO offsets in each iteration. Compared to the complicated SAGE algorithm, the proposed EFCE only requires $\mathcal{O}(Q^3 + NQ)$ operations.

VI. Conclusion

We have addressed the problem of timing and frequency synchronization in OFDM-based cooperative systems. To avoid multi-parameter and multi-dimensional search required by the exact ML estimator, we divided the subcarriers of the pilot OFDM block into tile subchannels and performed a correlation-type algorithm for timing synchronization and an ESPRIT-type algorithm, exploiting null subcarriers, for frequency synchronization. By judiciously choosing the tile size, it was shown that the proposed algorithms outperform the existing TDM based algorithm and SAGE algorithm significantly. The proposed algorithms are also computationally much more attractive than SAGE.

Appendix A
Derivation of equation (19-21)

We assume that subcarriers in a training sequence are uncorrelated and have the same power. Mathematically, this assumption implies that

$$\mathrm{E}\left\{X_m(k_1)X_m^*(k_2)\right\} = \frac{\sigma_{ts}^2}{VP}\delta_{k_1-k_2} \tag{27}$$

$$\mathrm{E}\left\{X_m(k_1)X_m(k_2)\right\} = 0 \tag{28}$$

where E is the statistical expectation operator and $\delta_{k_1-k_2}$ is the Kronecker delta. Since we assume that the noise is an AWGN with variance σ_v^2, we have that

$$\mathrm{E}\left\{\upsilon(n_1)\upsilon^*(n_2)\right\} = \sigma_\upsilon^2\delta_{n_1-n_2} \tag{29}$$

$$\mathrm{E}\left\{\upsilon(n_1)\upsilon(n_2)\right\} = 0 \tag{30}$$

Using eq. (27-30) and $P > L$, we readily obtain

$$\mathrm{E}\left\{|d_i(\tilde{\tau}_i + l)|^2\right\} = \sigma_{ts}^2\sigma_v^2 \tag{31}$$

$$\mathrm{E}\left\{|d_i(\tilde{\tau}_i + l)|^4\right\} = 2\sigma_{ts}^4 N\sigma_v^4 \tag{32}$$

$$\mathrm{E}\left\{|Z_{i,i}(\tilde{\tau}_i + l, 0)|^2\right\} = \xi(\varrho_l)\frac{\sigma_{ts}^4}{V^2}\mathrm{E}\left\{|h_i(\bar{\varrho}_l)|^2\right\} \tag{33}$$

$$\mathrm{E}\left\{|Z_{i,i}(\tilde{\tau}_i + l, 0)|^4\right\} = 2\xi^2(\varrho_l)\frac{\sigma_{ts}^8}{V^4}\mathrm{E}\left\{|h_i(\bar{\varrho}_l)|^2\right\}^2 \tag{34}$$

where $\varrho_l = \tilde{\tau}_i + l - \tau_i$, $\bar{\varrho}_l = \text{mod}(\varrho_l, P)$ and

$$\xi(\varrho_l) = \begin{cases} V^2 & 0 \le \varrho_l < P; \\ \left(\frac{\sin(\pi V n/Q)}{\sin(\pi n/Q)}\right)^2 & nP \le \varrho_l < (n+1)P; \end{cases} \tag{35}$$

$$\mathrm{E}\left\{|h_i(\bar{\varrho}_l)|^2\right\} = \sum_{k=0}^{L-1} \sigma^2_{h_i(k)} \delta_{k-\bar{\varrho}_l} \tag{36}$$

where $\sigma^2_{h_i(k)}$ is the power distribution of the kth channel tap of the ith relay. Following eq. (31-34), we have that

$$\mathrm{E}\left\{B(\tilde{\tau}_i + l)\right\} = \xi(\varrho_l)\frac{\sigma^4_{ts}}{V^2}\mathrm{E}\left\{|h_i(\bar{\varrho}_l)|^2\right\} + \sigma^2_{ts}\sigma^2_v \tag{37}$$

$$\begin{aligned}\mathrm{Var}\{B(\tilde{\tau}_i + l)\} = \xi^2(\varrho_l)\frac{\sigma^8_{ts}}{V^4}\mathrm{E}\left\{|h_i(\bar{\varrho}_l)|^2\right\}^2 + \\ 2\xi(\varrho_l)\frac{\sigma^6_{ts}}{V^2}\mathrm{E}\left\{|h_i(\bar{\varrho}_l)|^2\right\}\sigma^2_v + \sigma^4_{ts}N\sigma^4_v\end{aligned} \tag{38}$$

where $B(\tilde{\tau}_i + l) \triangleq |Z_{i,i}(\tilde{\tau}_i + l, 0) + d_i(\tilde{\tau}_i + l)|^2$. Eq. (39-42) can thus be readily obtained.

$$\mathrm{E}\left\{J(\tau_i) - J(\tau_i + n)\right\} = \sum_{l=0}^{L-1} \alpha_l \Big(\mathrm{E}\left\{B(\tau_i + l)\right\} - \mathrm{E}\left\{B(\tau_i + l + n)\right\}\Big) \tag{39}$$

$$\mathrm{Var}\{J(\tau_i) - J(\tau_i + 1)\} = \alpha_0^2\mathrm{Var}\{B(\tau_i)\} + \sum_{l=0}^{L-2}(\alpha_{l+1} - \alpha_l)^2\mathrm{Var}\{B(\tau_i + l + 1)\} + \alpha^2_{L-1}\mathrm{Var}\{B(\tau_i + L)\} \tag{40}$$

$$\mathrm{Var}\{J(\tau_i) - J(\tau_i - 1)\} = \alpha_0^2\mathrm{Var}\{B(\tau_i - 1)\} + \sum_{l=0}^{L-2}(\alpha_l - \alpha_{l+1})^2\mathrm{Var}\{B(\tau_i + l)\} + \alpha^2_{L-1}\mathrm{Var}\{B(\tau_i + L - 1)\} \tag{41}$$

$$\begin{aligned}\mathrm{Var}\{J(\tau_i) - J(\tau_i + nP)\} = \sum_{l=0}^{L-1} \alpha_l^2 \Big(\mathrm{Var}\{B(\tau_i + l)\} + 2\mathrm{E}\left\{B(\tau_i + l)\right\}\mathrm{E}\left\{B(\tau_i + l + nP)\right\} \\ + \mathrm{Var}\{B(\tau_i + l + nP)\} - 2\mathrm{E}\left\{B(\tau_i + l)B(\tau_i + l + np)\right\}\Big)\end{aligned} \tag{42}$$

where

$$\mathrm{E}\left\{B(\tau_i + l)B(\tau_i + l + np)\right\} = 2\xi(l + nP)\xi(l)\frac{\sigma^8_{ts}}{V^4}\mathrm{E}\left\{|h_i(l)|^2\right\}^2 + \left(\xi(l) + \xi(l + nP)\right)\frac{\sigma^6_{ts}}{V^2}\mathrm{E}\left\{|h_i(l)|^2\right\}\sigma^2_v + \sigma^4_{ts}\sigma^4_v$$

REFERENCES

[1] A. Sendonaris, E. Erkip, and B. Aazhang, "User cooperation diversity. Part I. System description," *IEEE Trans. Commun.*, vol. 51, no. 11, pp. 1927–1938, Nov. 2003.

[2] J. Laneman and G. Wornell, "Distributed space-time-coded protocols for exploiting cooperative diversity in wireless networks," *IEEE Trans. Inf. Theory*, vol. 49, no. 10, pp. 2415–2425, Oct. 2003.

[3] S. Jagannathan, H. Aghajan, and A. Goldsmith, "The effect of time synchronization errors on the performance of cooperative MISO systems," in *Proc. IEEE Global Telecommunications Conference Workshops GlobeCom Workshops 2004*, 29 Nov.-3 Dec. 2004, pp. 102–107.

[4] Y. Mei, Y. Hua, A. Swami, and B. Daneshrad, "Combating synchronization errors in cooperative relays," in *Proc. IEEE International Conference on Acoustics, Speech, and Signal Processing*, vol. 3, 18-23 Mar. 2005, pp. 369–372.

[5] Z. Li and X. Xia, "A Simple Alamouti Space-Time Transmission Scheme for Asynchronous Cooperative Systems," *Signal Processing Letters, IEEE*, vol. 14, no. 11, pp. 804–807, Nov. 2007.

[6] F. Ng and X. Li, "Cooperative STBC-OFDM Transmissions with Imperfect Synchronization in Time and Frequency," in *Conference Record of the Thirty-Ninth Asilomar Conference on Signals, Systems and Computers*, 28 Oct.-1 Nov. 2005, pp. 524–528.

[7] M.-K. Oh, X. Ma, G. Giannakis, and D.-J. Park, "Cooperative synchronization and channel estimation in wireless sensor networks," in *Conference Record of the Thirty-Seventh Asilomar Conference on Signals, Systems and Computers*, vol. 1, 9-12 Nov. 2003, pp. 238–242.

[8] J.-J. van de Beek, P. Borjesson, M.-L. Boucheret, D. Landstrom, J. Arenas, P. Odling, C. Ostberg, M. Wahlqvist, and S. Wilson, "A time and frequency synchronization scheme for multiuser OFDM," *IEEE J. Sel. Areas Commun.*, vol. 17, no. 11, pp. 1900–1914, Nov. 1999.

[9] M. Morelli, "Timing and frequency synchronization for the uplink of an OFDMA system," *IEEE Trans. Commun.*, vol. 52, no. 2, pp. 296–306, Feb. 2004.

[10] M.-O. Pun, M. Morelli, and C.-C. Kuo, "Maximum-likelihood synchronization and channel estimation for OFDMA uplink transmissions," *IEEE Trans. Commun.*, vol. 54, no. 4, pp. 726–736, Apr. 2006.

[11] J.-H. Lee and S.-C. Kim, "Time and Frequency Synchronization for OFDMA Uplink System using the SAGE Algorithm," *IEEE Trans. Wireless Commun.*, vol. 6, no. 4, pp. 1176–1181, Apr. 2007.

[12] A. Saemi, J.-P. Cances, and V. Meghdadi, "Synchronization algorithms for MIMO OFDMA systems," *IEEE Trans. Wireless Commun.*, vol. 6, no. 12, pp. 4441–4451, Dec. 2007.

[13] Z. Cao, U. Tureli, and Y. Yao, "Deterministic multiuser carrier-frequency offset estimation for interleaved OFDMA uplink," *IEEE Trans. Commun.*, vol. 52, no. 9, pp. 1585–1594, Sep. 2004.

[14] J. Lee, S. Lee, K.-J. Bang, S. Cha, and D. Hong, "Carrier Frequency Offset Estimation Using ESPRIT for Interleaved OFDMA Uplink Systems," *IEEE Trans. Veh. Technol.*, vol. 56, no. 5, pp. 3227–3231, Sep. 2007.

[15] T. Schmidl and D. Cox, "Robust frequency and timing synchronization for OFDM," *IEEE Trans. Commun.*, vol. 45, no. 12, pp. 1613–1621, Dec. 1997.

[16] H. Minn, V. Bhargava, and K. Letaief, "A robust timing and frequency synchronization for OFDM systems," *IEEE Trans. Wireless Commun.*, vol. 2, no. 4, pp. 822–839, Jul. 2003.

[17] M. Ghogho and A. Swami, "Frame and Frequency Acquisition for OFDM," *Signal Processing Letters, IEEE*, vol. 15, pp. 605–608, 2008.

[18] M. Morelli and U. Mengali, "An improved frequency offset estimator for OFDM applications," *Communications Letters, IEEE*, vol. 3, no. 3, pp. 75–77, Mar. 1999.

[19] M. Ghogho, P. Ciblat, A. Swami, and P. Bianchi, "Training Design for Repetitive-Slot-based CFO estimation in OFDM," *IEEE Trans. Signal Process.*, vol. xx, no. xx, pp. xxx–xxx, Forthcoming 2009.

[20] M. Ghogho, A. Swami, and G. Giannakis, "Optimized null-subcarrier selection for CFO estimation in OFDM over

frequency-selective fading channels," in *Proc. IEEE Global Telecommunications Conference*, vol. 1, 25-29 Nov. 2001, pp. 202–206.

[21] R. Bachl, "The forward-backward averaging technique applied to TLS-ESPRIT processing," *IEEE Trans. Signal Process.*, vol. 43, no. 11, pp. 2691–2699, Nov. 1995.

[22] X. Y. Fu and H. Minn, "Initial uplink synchronization and power control (ranging process) for OFDMA systems," in *Proc. IEEE Global Telecommunications Conference*, vol. 6, 29 Nov.-3 Dec. 2004, pp. 3999–4003.

[23] E. Zhou, H. Zhao, and W. B. Wang, "Timing Synchronization for Interleaved OFDMA Uplink System," in *Proc. International Conference on Communications, Circuits and Systems*, vol. 2, 25-28 Jun. 2006, pp. 1147–1152.

[24] P. Stoica and N. Arye, "MUSIC, maximum likelihood, and Cramer-Rao bound," *Acoustics, Speech, and Signal Processing [see also IEEE Transactions on Signal Processing], IEEE Transactions on*, vol. 37, no. 5, pp. 720–741, May 1989.

Practical timing and frequency synchronization for OFDM based cooperative systems

Qinfei Huang, Mounir Ghogho, Jibo Wei and Philippe Ciblat

***Abstract*—In this paper, we investigate the timing and carrier frequency offset (CFO) synchronization problem in decode and forward cooperative systems operating over frequency selective channels. A training sequence which consists of *one* OFDM block having a *tile* structure in the frequency domain is proposed to perform synchronization. Timing offsets are estimated using correlation-type algorithms. By inserting some null subcarriers in the proposed tile structure, we propose a computationally efficient subspace decomposition-based algorithm for CFO estimation. The issue of optimal tile length is studied both theoretically and through simulations. By judiciously designing the tile size of the pilot, the proposed algorithms are shown to have better performance, in terms of synchronization errors and bit error rate, than the time-division multiplexing-based training method and the computationally demanding SAGE algorithm.**

***Index Terms*—Timing estimation, CFO estimation, OFDM, cooperative systems**

I. Introduction

Multiple-input and multiple-output (MIMO) system is a well-known technique to increase the capacity and diversity of wireless communications. However, due to the limitations on the hardware or cost, equipping devices with multiple antennas may not be possible in some wireless networks. For this reason, a class of techniques known as cooperative communication has been introduced [1] [2]. The basic principle is to construct a virtual multiple-antenna system by sharing antennas of neighboring users in a distributed manner. The same benefits of multiple-antenna systems can be achieved in a cooperative system with proper cooperative strategies.

Different from MIMO systems, multiple nodes in these cooperative systems are not only distributed in space but also have their own oscillators, which means that there are multiple timing offsets and frequency offsets in cooperative transmission. These offsets may drastically undermine the diversity potential of cooperative networks, see e.g. [3]. OFDM-based cooperative schemes have recently been proposed to combat timing errors (see e.g. [4] and [5].) Indeed, with a cyclic prefix (CP) insertion, OFDM is robust to limited timing errors. However, without compensation for the timing offsets, each OFDM block needs to employ an unnecessarily long CP to mitigate the interblock/multinode interference [6]. This can significantly reduce the data throughput, especially when the expected timing errors are large. Timing synchronization for all the relay nodes is therefore desirable to overcome this problem. Further, OFDM systems are very sensitive to carrier-frequency offsets (CFO). Therefore, accurate timing and frequency synchronization is key for the deployment of efficient OFDM-based cooperative systems.

To avoid the multidimensional search required by maximum-likelihood (ML) synchronization, a time division multiplexing (TDM) training based synchronization algorithm was proposed in [7]. However, although the resulting algorithms are computationally attractive, the overhead is extremely high since long guard time intervals may be required to avoid overlap of different relay node signals, especially in mobile networks where the assignment of relay nodes can be highly dynamic. A solution to obtain a good tradeoff between computational complexity and overhead is to multiplex different relay node training signals in the frequency domain. The synchronization problem then becomes similar to that in uplink OFDMA systems. Thus, synchronization algorithms for uplink OFDMA may in principle be applied to our problem. However, subband methods proposed in [8] prevents the possibility of optimally exploiting the channel diversity, and most of the other existing algorithms need to perform a complicated iterative search to estimate the timing and frequency offsets (see e.g. [9]–[12] and references therein). Further, iterative-type algorithms are sensitive to initialization. Finally and more importantly, in uplink OFDM, the received signals are processed by the base station which can afford running complex algorithms, whereas in cooperative systems, the receiver may be a mobile unit for which the computational complexity and power consumption are critical issues.

In this paper, we show that synchronization algorithms with low computational complexity and good performance can be achieved with a single OFDM training block having a *tile* structure in the frequency domain. Timing offsets are estimated using correlation-type algorithms. The CFOs are estimated using null-subcarriers inserted in the tile structure and an ESPRIT-type algorithm. By judiciously designing the size of the tile, these low-complexity algorithms are shown to have better performance, in terms of synchronization errors and bit error rate, than the computationally demanding SAGE algorithm. Unlike [13] and [14] which only consider CFO estimation for the interleaved OFDMA uplink, both timing and frequency estimation are investigated in this paper.

The rest of paper is organized as follows. In Section II, a brief introduction of the decode and forward cooperative system model and tile-based training structure are presented. Synchronization algorithms are proposed in Section III. Performance analysis of the proposed algorithms is investigated in IV and verified via simulation in Section V. Finally, some conclusions are drawn in Section VI.

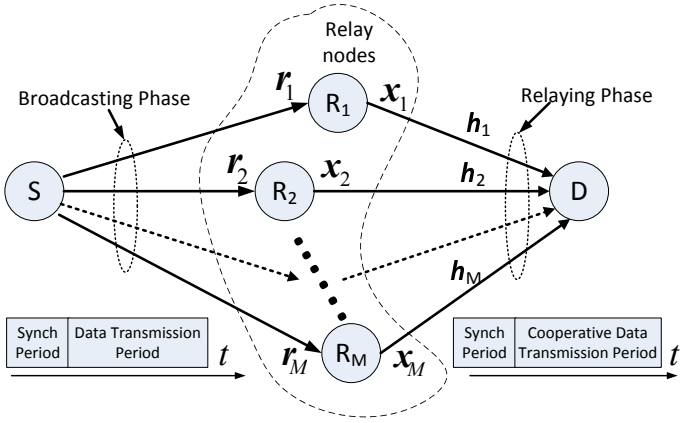

Fig. 1. Cooperative system structure

II. Cooperative system model

A. System description

We consider a decode and forward cooperative system with one source node, one destination node and M relay nodes as shown in Fig. 1. Training sequences are used for synchronization.

In the broadcasting phase, the source node broadcasts a training sequence followed by data blocks to the relay nodes. Each relay node operates independently. In the relaying phase, during the synchronization period, the M relay nodes transmit training sequences to the destination node. A multiple parameter estimation task is performed at the destination node. As discussed in [9], accurate timing and frequency compensation cannot be accomplished at the destination node, as the correction of one relay node's offsets would misalign the other relay nodes. To overcome this problem, the destination node may feed back the estimated offsets to the relay nodes. Then, each node can adjust its timing and frequency parameters, so that the data blocks can arrive in a synchronous manner at the destination node. Asynchronous data detection can also be carried out but its complexity may be too high for mobile nodes. It is also worth pointing out that asynchronism may provide delay diversity for flat fading channels but it may have little value in the case of frequency-selective channels. To assess the merits of our synchronization algorithm in terms of bit error rate, we consider in our simulation setup the scenario where relay nodes are synchronized using feedback from the destination node and data transmission from the relay nodes is performed using cooperative space-time block coding.

The synchronization problem in the broadcasting phase is similar to that of a downlink OFDMA, for which single user OFDM synchronization techniques (see e.g. [15]–[17] and references therein) can be applied. Hence, we focus on the relaying phase, which is more challenging than the broadcasting phase. In principle, if the relay nodes perfectly synchronize to the source node in the broadcasting phase, the synchronization problem in the relaying phase would be simpler because there would be only one CFO to be estimated (but still multiple delay offsets). However, in practical wireless networks, synchronization is never perfect and offsets may vary over time due to node mobility and oscillator drifts.

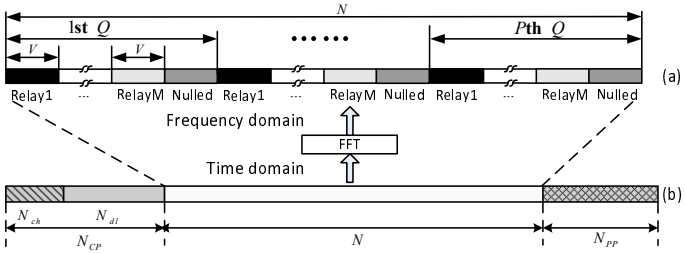

Fig. 2. Training structure illustration

B. Training sequence structure and receive signal model

The training sequence for each node consists of a useful part, a cyclic prefix (CP) and a cyclic postfix (PP). As in [13], the CP is composed of two parts of lengths N_{ch} and N_{dl}. The N_{ch} sample-long part of the CP is dedicated to accommodating the channel delay spreads, and the N_{dl} sample-long parts of the CP and the PP, whose length is denoted by N_{pp}, are inserted to accommodate the different propagation delays among relay nodes. It is worth pointing out that the proposed training sequences introduce a lower overhead than the TDM training sequences adopted in [7], since long guard time intervals are required by each TDM training sequence. The structure of the proposed training sequence is shown in Fig. 2.b. In this paper, we assume that the normalized CFO is less than half of the subcarrier spacing ($|\omega_i| < 0.5$) and the maximum differential propagation delay $\max\{|\tau_i - \tau_j|\}$ is smaller than $\min\{N_{dl}, N_{pp}\}$.

The useful part of the training sequence (i.e. excluding CP and PP) for each relay node consists of one OFDM block of DFT size N. The activated subcarriers are distributed among the relay nodes as follows. As depicted in Fig. 2.a, the N subcarriers are divided into P groups and each group contains Q subcarriers; P is set to be larger than the length of channel taps in order to be able to perform channel estimation. A *tile subchannel* is composed by V adjacent subchannels of each group. Parameter V will be referred to as the *tile size*. The number of subcarriers allocated to all the relay nodes in each group is set to be smaller than Q, i.e. $MV < Q$, so that null subcarriers, to be used for CFO estimation, can be inserted. The tile subchannel assigned to the ith relay node is composed of subcarriers with index set $\mathcal{M}_i = \{\eta_{i,v,p} = v + pQ + (i-1)V, v = 0, ..., V-1; p = 0, ..., P-1\}$. Letting $\boldsymbol{X}_i = [X_i(0) \cdots X_i(N-1)]^T$ and $\boldsymbol{x}_i = [x_i(0) \cdots x_i(N-1)]^T$ respectively denote the frequency and time domain training sequences of the ith user, we have that

$$x_i(n) = \frac{1}{\sqrt{N}} \sum_{v=0}^{V-1} \sum_{p=0}^{P-1} X_i(\eta_{i,v,p}) e^{j2\pi\eta_{i,v,p}n/N}, \quad n = 0, \cdots, N-1 \tag{1}$$

After adding the CP, the transmitted training sequences can be expressed as

$$x_i(n) = \begin{cases} x_i(N+n) & n = -1, \cdots, -N_{cp} \\ x_i(n) & n = 0, \cdots, N-1 \\ x_i(n-N) & n = N, \cdots, N+N_{pp-1} \end{cases}$$

Removing the CP and collecting the first N samples, the received version of the training signal at the destination node can be written as

$$r(n) = \sum_{i=1}^{M} e^{j2\pi\omega_i n/N} \sum_{l=0}^{L-1} h_i(l) x_i(n-l-\tau_i) + \upsilon(n), \quad n = 0, \cdots, N-1 \tag{2}$$

where $\boldsymbol{h}_i = [h_i(0) \cdots h_i(L-1)]^T$, τ_i and ω_i are respectively the channel impulse response (CIR), the integer part of the normalized (to the sampling period) delay and the normalized (to the inverse of the symbol period) CFO associated with the ith relay node, and $\upsilon(n)$ is an AWGN with variance σ_υ^2. Since OFDM modulation is used, the fractional part of the propagation delay and initial phase are not explicitly included in the above signal model because they can be incorporated into the channel frequency response.

Letting $\boldsymbol{r} = [r(0) \cdots r(N-1)]^T$, $\boldsymbol{\Gamma}(\omega_i) = \text{diag}\{1, e^{j2\pi\omega_i/N}, \cdots, e^{j2\pi\omega_i(N-1)/N}\}$; $[\mathbf{X}_{\tau_i}]_{m,n} = x_i(m-n-\tau_i)$, where $m = 0, \cdots, N-1$ and $n = 0, \cdots, L-1$, and $\boldsymbol{\upsilon} = [\upsilon(0) \cdots \upsilon(N-1)]^T$, vector $\boldsymbol{r}$ can, using Eq (2), be expressed as

$$\boldsymbol{r} = \mathbf{A}_{\boldsymbol{\omega},\boldsymbol{\tau}} \boldsymbol{h} + \boldsymbol{\upsilon} \tag{3}$$

where $\mathbf{A}_{\boldsymbol{\omega},\boldsymbol{\tau}} = [\boldsymbol{\Gamma}(\omega_1)\mathbf{X}_{\tau_1}, \cdots, \boldsymbol{\Gamma}(\omega_M)\mathbf{X}_{\tau_M}]$; $\boldsymbol{h} = [\boldsymbol{h}_1^T \cdots \boldsymbol{h}_M^T]^T$; $\boldsymbol{\omega} = [\omega_1, \cdots, \omega_M]^T$; $\boldsymbol{\tau} = [\tau_1, \cdots, \tau_M]^T$.

The joint ML estimators of the timing and CFO parameters can be readily expressed as

$$(\hat{\boldsymbol{\tau}}, \hat{\boldsymbol{\omega}}) = \arg\max_{\boldsymbol{\tau},\boldsymbol{\omega}} \left\{ \boldsymbol{r}^H \mathbf{A}_{\boldsymbol{\omega},\boldsymbol{\tau}} \left(\mathbf{A}_{\boldsymbol{\omega},\boldsymbol{\tau}}^H \mathbf{A}_{\boldsymbol{\omega},\boldsymbol{\tau}} \right)^{-1} \mathbf{A}_{\boldsymbol{\omega},\boldsymbol{\tau}}^H \boldsymbol{r} \right\}. \tag{4}$$

The maximization in (4) requires a search over the $2M$ dimensional domain spanned by $(\boldsymbol{\omega}, \boldsymbol{\tau})$, which may not be tractable in practice. Unlike [7] which uses a TDM training sequence to avoid the multidimensional search, we adopt a frequency-domain multiplexing for our training design in order to obtain low overhead.

III. Timing and Frequency Offsets Estimation

A. Timing offsets estimation algorithm

In this subsection, we present a Weighted Slide Cross-correlation Timing Estimator (WSCTE), which can estimate each relay node timing parameter readily and accurately by exploring the cross correlation between the received signal and each relay node's training sequence.

Using the above training structure, the received signal can be re-expressed as

$$r(n) = \sum_{i=1}^{M} r^{(i)}(n) + \upsilon(n), \ n = 0, \cdots, N-1 \tag{5}$$

where $r^{(i)}(n) = \sum_{v=0}^{V-1} r^{(i,v)}(n)$ and

$$r^{(i,v)}(n) = \frac{1}{\sqrt{N}} e^{j\phi_i} e^{j\theta_{i,v}(n-\tau_i)} \sum_{p=0}^{P-1} X_i(\eta_{i,v,p}) H_i(\eta_{i,v,p}) e^{j2\pi p(n-\tau_i)/P} \tag{6}$$

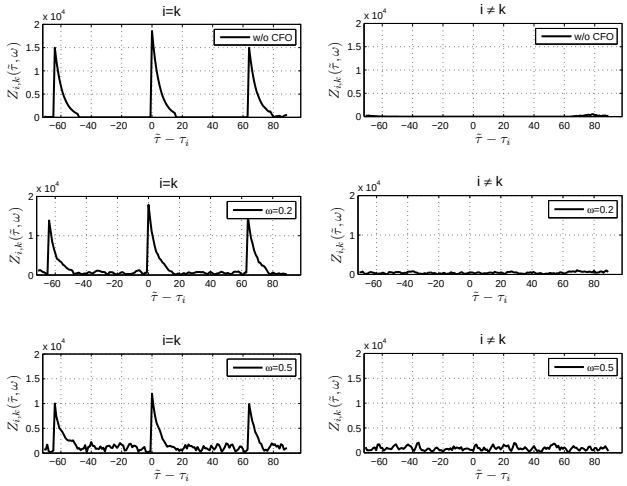

Fig. 3. $Z_{i,k}(\tilde{\tau}, \omega_i)$ versus $\tilde{\tau} - \tau_i$ for different values of ω_i; $N = 512$, $L = 16$, $V = 3$, $Q = 8$

where $\phi_i = 2\pi\omega_i\tau_i/N$; $\theta_{i,v} = 2\pi(\omega_i + v + (i-1)V)/N$ is a CFO-related parameter, and $H_i(k)$ is the channel frequency response at the kth subcarriers of the ith relay node.

Let $Z_{i,k}(\tilde{\tau}, \omega_i) \triangleq \sum_{n=0}^{N-1} r^{(i)}(n+\tilde{\tau}) x_k^*(n)$. Using eq. (6), we get

$$Z_{i,k}(\tilde{\tau}, \omega_i) = \begin{cases} 0 & i \neq k, \ \omega_i = 0; \\ Q \sum_{v_1=v_2=0}^{V-1} Y_{i,i}(\tilde{\tau}, 0) & i = k, \ \omega_i = 0; \\ \sum_{v_1=0}^{V-1} \sum_{v_2=0}^{V-1} \epsilon_{i,k}(\omega_i) Y_{i,k}(\tilde{\tau}, \omega_i) & \omega_i \neq 0 \end{cases} \tag{7}$$

where $\epsilon_{i,k}(\omega_i) \triangleq \frac{1-e^{j2\pi\omega_i}}{1-e^{j2\pi(\rho_{i,v_1} - \rho_{k,v_2} + \omega_i)/Q}}$, $\rho_{i,v} = v + (i-1)V$ and

$$Y_{i,k}(\tilde{\tau}, \omega_i) \triangleq \frac{1}{N} e^{j\phi_i} \sum_{n=0}^{P-1} e^{-j\theta_{i,v_1}(\tau_i - \tilde{\tau})} e^{j2\pi(\rho_{i,v_1} - \rho_{k,v_2} + \omega_i)n/N} g_{i,v_1}(n - \tau_i + \tilde{\tau}) f_{k,v_2}^*(n)$$

where $f_{i,v}(n) \triangleq \sum_{p=0}^{P-1} X_i(\eta_{i,v,p}) e^{j2\pi np/P}$, $g_{i,v}(n) \triangleq \sum_{p=0}^{P-1} X_i(\eta_{i,v,p}) H_i(\eta_{i,v,p}) e^{j2\pi np/P}$, and $*$ denotes the complex conjugate operator.

It can be deduced from the first and second terms in the RHS of eq. (7) that the received signal has good correlation properties. However, in the presence of CFO, the above results do not hold anymore. Nevertheless, since the normalized CFO is assumed to be less than half of the subcarriers spacing, it can be verified that the effect of the CFO can be neglected as shown in Fig. 3. Exploiting multipath diversity, the proposed WSCTE algorithm is given by

$$\hat{\tau}_i = \arg\max_{\tilde{\tau}_i} J(\tilde{\tau}_i) \tag{8}$$

where

$$J(\tilde{\tau}_i) = \sum_{l=0}^{L-1} \alpha_l \left| \sum_{n=0}^{N-1} r(n+\tau_i+l) x_i^*(n) \right|^2 \tag{9}$$

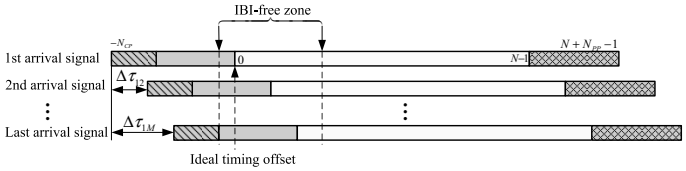

Fig. 4. Illustration of interblock-interference-free zone for timing offset estimation error

and $\boldsymbol{\alpha} = [\alpha_0 \ \cdots \ \alpha_{L-1}]^T$ are weighting coefficients, whose optimal design will be addressed later.

B. CFOs estimation algorithm

Once the timing offset estimation is carried out, we collect samples of the received signal as follows. The starting point of this set of samples is determined by the estimated timing parameter of the relay node whose signal arrives first at the destination. We assume that the timing offset estimation error of the first arrival signal is within the interblock-interference-free zone, $[-N_{CP} + \Delta\tau_{1M} + N_{ch},\ N_{PP} - 1]$, as shown in Fig. 4, where $\Delta\tau_{1M}$ denotes the timing offset between the first and last arriving signals, so that the receive signal at the destination node still has a per-component repetitive structure. Let $\{\tilde{r}(n)\}_{n=0}^{N-1}$ denote the collected N samples after timing offset estimation. From eq. (5), we get

$$\tilde{r}(n+\mu P) = \sum_{i=1}^{M}\sum_{v=0}^{V-1} e^{j\theta_{i,v}\mu P}\tilde{r}^{(i,v)}(n) + v(n+\mu P) \quad n = 0,\cdots,P-1,\ \mu = 0,\cdots,Q-1 \tag{10}$$

We then arrange the N samples into a $Q \times P$ matrix

$$\mathbf{R} = \begin{bmatrix} \tilde{r}(0) & \cdots & \tilde{r}(P-1) \\ \tilde{r}(P) & \cdots & \tilde{r}(2P-1) \\ \vdots & \ddots & \vdots \\ \tilde{r}((Q-1)P) & \cdots & \tilde{r}(N-1) \end{bmatrix}_{Q\times P} \tag{11}$$

Letting $\boldsymbol{R}_p$ denote the pth column of matrix $\mathbf{R}$, we have that

$$\boldsymbol{R}_p = \mathbf{G}\tilde{\boldsymbol{r}}_p + \boldsymbol{v}_p,\ l = 0,\cdots,P-1 \tag{12}$$

where $\tilde{\boldsymbol{r}}_p = \left[\tilde{r}^{(1,0)}(p)\ \tilde{r}^{(1,1)}(p)\ \cdots\ \tilde{r}^{(M,V-1)}(p)\right]^T$ and $\mathbf{G}$ is a $(Q \times MV)$ matrix given by

$$\mathbf{G} = \begin{bmatrix} 1 & 1 & \cdots & 1 \\ e^{j\theta_{1,0}P} & e^{j\theta_{1,1}P} & \cdots & e^{j\theta_{M,V-1}P} \\ \vdots & \vdots & \ddots & \vdots \\ e^{j\theta_{1,0}(Q-1)P} & e^{j\theta_{1,1}(Q-1)P} & \cdots & e^{j\theta_{M,V-1}(Q-1)P} \end{bmatrix}$$

The main idea behind the proposed low-complexity CFO estimation algorithm is to first estimate the $\theta_{i,v}$'s, which are distinct from each other since the ω_i's are assumed to be less than 0.5 in absolute value, and then appropriately combine estimates of the $\theta_{i,v}$'s to obtain the CFO estimates. This approach allows us to estimate the multiple CFOs using *one* OFDM symbol. Indeed, the $\theta_{i,v}$'s in eq. (10) cause phase shifts to identical P-sample long segments. Hence, our approach can in a way be seen as an extension of the repetitive-slot CFO estimation approach (see e.g. [18], [19]) to the case of multiple CFO estimation.

Once we express the received samples as in eq. (10), CFO estimation can be carried out using a signal subspace decomposition approach. The dimension of the null subspace is dictated by the number of null subcarriers, which is equal to $Q - MV$. CFO estimation for single user OFDM using null subcarriers was studied in e.g. [20] and references therein. Thus, to estimate the multiple CFOs, subspace based methods (MUSIC and ESPRIT) are known to provide low complexity algorithms, compared to the ML method. Here we adapt one of the modified versions of ESPRIT, namely forward-backward smoothing ESPRIT (FBS-ESPRIT) [21] to our CFO estimation problem.

The multiple CFOs are estimated using the following steps:

Step 1) Arrange the received signal $\tilde{\boldsymbol{r}}$ into matrix $\mathbf{R}$.

Step 2) The covariance matrix $\boldsymbol{\Omega} = \mathrm{E}\left\{\boldsymbol{R}_p\boldsymbol{R}_p^H\right\}$ of $\boldsymbol{R}_p$ is estimated by using the forward-backward smoothing principle as

$$\widehat{\boldsymbol{\Omega}} = \frac{1}{2}\left(\tilde{\boldsymbol{\Omega}} + \mathbf{J}\tilde{\boldsymbol{\Omega}}^T\mathbf{J}\right)$$

where $\tilde{\boldsymbol{\Omega}} = \frac{1}{P}\mathbf{R}\mathbf{R}^H$ and $\mathbf{J}$ is the exchange matrix with 1's on the anti-diagonal and 0's elsewhere.

Step 3) Compute singular value decomposition (SVD) of $\widehat{\boldsymbol{\Omega}}$, and arrange the eigenvectors of $\widehat{\boldsymbol{\Omega}}$ that are associated to the MV largest eigenvalues $\lambda_1 \geq \lambda_2 \geq \cdots \geq \lambda_{MV}$ into a $Q \times MV$ matrix $\mathbf{U}_s$. Let $\mathbf{U}_{s1}$ denote the first $(Q-1)$ rows of $\mathbf{U}_s$ and $\mathbf{U}_{s2}$ denote the last $(Q-1)$ rows of $\mathbf{U}_s$. The $\theta_{i,v}$'s are estimated as

$$\hat{\theta}_{i,v} = \frac{1}{P}\arg(\beta_k), \qquad k = v + (i-1)V \tag{13}$$

where $\{\beta_k\}_{k=0}^{MV-1}$ are the eigenvalues of

$$\boldsymbol{\Xi} = \left(\mathbf{U}_{s1}^H\mathbf{U}_{s1}\right)^{-1}\mathbf{U}_{s1}^H\mathbf{U}_{s2}$$

.

Step 4) After getting the $\hat{\theta}_{i,v}$'s, we adopt, for simplicity, equal gain combining (EGC) to compute the CFO estimate for each relay node. Thus, the proposed EGC-FBS-ESPRIT-based CFO estimator, which will be referred to as EFCE, is given by

$$\hat{\omega_i} = \frac{1}{V}\sum_{v=0}^{V-1}\left(\frac{N\hat{\theta}_{i,v}}{2\pi} - v\right) - i + 1,\ i = 1,\cdots,M \tag{14}$$

Another subspace-based methods (Spectral MUSIC and total least square ESPRIT) has been applied to the interleaved OFDMA uplink system in [13] and [14]. However, it is worth pointing out that the interleaved subcarriers allocation is a special case ($V = 1$) of the proposed pilot structure. We will see later that $V = 1$ is not a good choice.

IV. Performance Analysis

Since timing and frequency offsets are respectively discrete and continuous parameters, it is complicated to analyze the timing and frequency offsets estimation performance jointly. Therefore, we investigate the performance of the proposed estimation algorithms, WSCTE and EFCE, separately.

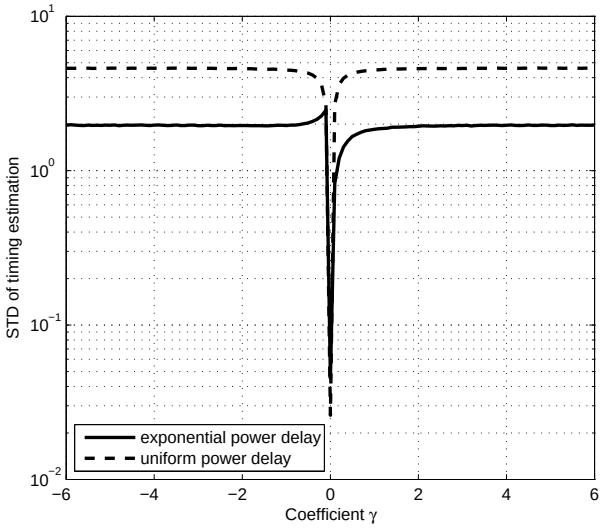

Fig. 5. γ Versus standard deviation of timing estimation, $N = 512$, $L = 16$, $M = 2$, $V = 3$, $Q = 8$, SNR=20dB

A. WSCTE weights selection

From eq. (8), the optimal weights can be obtained by optimizing the following equation

$$\boldsymbol{\alpha}^o = \arg\max_{\boldsymbol{\alpha}} \Pr(J(\tilde{\tau}_i = \tau_i) > J(\tilde{\tau}_i \neq \tau_i)|\boldsymbol{\alpha}) \tag{15}$$

under the constraint $\sum_{l=0}^{L-1} \alpha_l = 1$, where $\Pr(a|b)$ denotes the conditional probability. However, since the $J(\tilde{\tau}_i)$'s are dependent Gamma distributed variables, it is cumbersome to derive a close-form expression for the conditional probability. Hence, a numerical suboptimal solution is desired.

We consider a class of weights which satisfy $\alpha_l = C_\gamma e^{-\gamma l}$, where $\gamma = (-\infty, +\infty)$ and C_γ is a scalar factor that ensures that the sum of all weights is normalized to unity. It is worth pointing out that $\boldsymbol{\alpha}$ approximates $[1, 0, \cdots, 0]^T$ for sufficiently large positive γ, which is the weight vector used in [22], [23]. We will show that the performance of WSCTE can be much improved by judiciously selecting the weights.

To simplify the performance analysis of timing estimation, we consider the case without CFOs in this and the following subsections. It is worth pointing out that the results hold true even in the presence of CFO values considered in this paper. Fig. 5 shows the standard deviation of WSCTE versus various γ. Both the exponential power delay profile, i.e. $\left(\mathrm{E}\left\{|h_i(l)|^2\right\}_{l=0}^{L-1} = C\exp(-0.2l) \right.$ where C is a scalar factor that ensures that the total energy of the channel taps is normalized to unity) and the uniform power delay $\left(\mathrm{E}\left\{|h_i(l)|^2\right\}_{l=0}^{L-1} = 1/L\right)$ profile have been tested. Fig. 5 clearly shows that $\gamma = 0$ gives the best estimation performance among all examined values of γs. Hence, $\boldsymbol{\alpha} = [1, \cdots, 1]^T/L$ is adopted in this paper.

B. Tile size selection for WSCTE

We define the optimal tile size for WSCTE as the value of V that maximizes the probability of exact determination of the delays, i.e.

$$V^o = \arg\max_{V} \Pr(J(\tilde{\tau}_i = \tau_i) > J(\tilde{\tau}_i \neq \tau_i)|V) \tag{16}$$

As for eq. (15), it is analytically untractable to solve the above optimization problem. As shown in Fig. 3, we can notice that a wrong estimate of τ_i will most likely be in the set $\{\tau_i \pm 1, \tau_i \pm P\}$. Thus, we simplify the above optimization problem as follows

$$V^o = \arg\min_{V} \sum_{n=1}^{4} \Pr_n(V) \tag{17}$$

where $\Pr_1(V) = \Pr(J(\tilde{\tau}_i = \tau_i) < J(\tilde{\tau}_i = \tau_i + 1)|V)$; $\Pr_2(V) = \Pr(J(\tilde{\tau}_i = \tau_i) < J(\tilde{\tau}_i = \tau_i - 1)|V)$; $\Pr_3(V) = \Pr(J(\tilde{\tau}_i = \tau_i) < J(\tilde{\tau}_i = \tau_i + P)|V)$ and $\Pr_4(V) = \Pr(J(\tilde{\tau}_i = \tau_i) < J(\tilde{\tau}_i = \tau_i - P)|V)$.

Without CFOs, eq. (9) can be rewritten as

$$J(\tilde{\tau}_i) = \sum_{l=0}^{L-1} \alpha_l \left| Z_{i,i}(\tilde{\tau}_i + l, 0) + d_i(\tilde{\tau}_i + l) \right|^2 \tag{18}$$

where $d_i(\tilde{\tau}_i + l) = \sum_{n=0}^{N-1} \upsilon(n + \tilde{\tau}_i + l) x_i^*(n)$. We assume that the training sequences of different relay nodes are uncorrelated and power constrained, i.e. $\sum_{n=0}^{N-1} |X_i(n)|^2 = \sigma_{ts}^2$. Using $\boldsymbol{\alpha} = [1, \cdots, 1]^T/L$ as weights and after some tedious manipulation (see Appendix A), for high SNR, we obtain

$$\begin{aligned} \mathrm{E}\left\{J(\tau_i) - J(\tau_i + 1)\right\} &= \frac{\sigma_{ts}^4}{L} \mathrm{E}\left\{|h_i(0)|^2\right\} \\ \mathrm{Var}\{J(\tau_i) - J(\tau_i + 1)\} &= \frac{\sigma_{ts}^8}{L^2} \mathrm{E}\left\{|h_i(0)|^2\right\}^2 \end{aligned} \tag{19}$$

$$\begin{aligned} \mathrm{E}\left\{J(\tau_i) - J(\tau_i - 1)\right\} &= \frac{\sigma_{ts}^4}{L} \mathrm{E}\left\{|h_i(L-1)|^2\right\} \\ \mathrm{Var}\{J(\tau_i) - J(\tau_i - 1)\} &= \frac{\sigma_{ts}^8}{L^2} \mathrm{E}\left\{|h_i(L-1)|^2\right\}^2 \end{aligned} \tag{20}$$

$$\begin{aligned} \mathrm{E}\left\{J(\tau_i) - J(\tau_i \pm P)\right\} &= \frac{\sigma_{ts}^4}{LV^2}(V^2 - \xi(\pm P)) \\ \mathrm{Var}\{J(\tau_i) - J(\tau_i \pm P)\} &= \frac{\sigma_{ts}^8}{L^2V^4}(V^2 - \xi(\pm P))^2 \\ &\quad \sum_{l=0}^{L-1} \mathrm{E}\left\{|h_i(l)|^2\right\}^2 \end{aligned} \tag{21}$$

where $\xi(\pm P)$ is defined in eq. (35) in the appendix. The following remarks are in order.

1) $\Pr_1(V)$ and $\Pr_2(V)$ are independent of V.
2) For $V = 1$, we have that $\mathrm{E}\left\{J(\tau_i) - J(\tau_i \pm P)\right\} = 0$ and $\mathrm{Var}\{J(\tau_i) - J(\tau_i \pm P)\} = 0$, which means that $V = 1$ causes ambiguities in timing estimation. These ambiguities vanish for larger values of V.
3) Since the coefficient of variation of $J(\tau_i) - J(\tau_i \pm P)$, defined as $\sqrt{\mathrm{Var}\{J(\tau_i) - J(\tau_i \pm P)\}}/\mathrm{E}\left\{J(\tau_i) - J(\tau_i \pm P)\right\}$, is independent of V for $V > 1$, the dispersion of $J(\tau_i) - J(\tau_i \pm P)$ is independent of V and larger $\mathrm{E}\left\{J(\tau_i) - J(\tau_i \pm P)\right\}$ will give smaller $\Pr_3(V)$ and $\Pr_4(V)$.

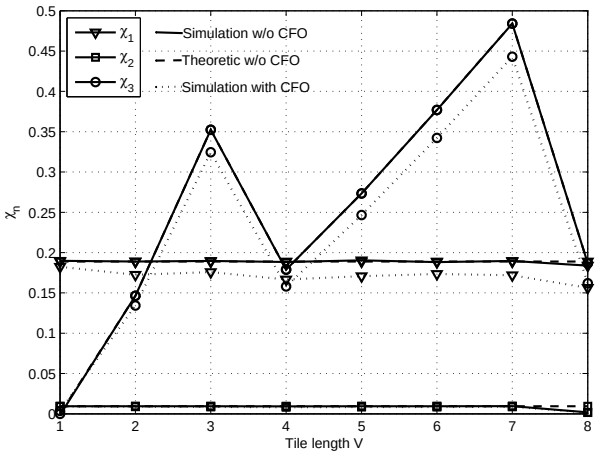

Fig. 6. χ_n Versus tile size V, $N = 512$, $L = 16$, $M = 2$, $Q = 2^{\lfloor \log_2 MV \rfloor + 1}$, SNR=20dB, CFO case $\omega_1 = \omega_2 = 0.5$

4) The optimal V can be approximated by

$$V^o \approx \arg\max_V \{\sum_{i=1}^{4} \chi_i\} \tag{22}$$

where $\chi_1 = \mathrm{E}\{J(\tau_i) - J(\tau_i + 1)\}/\mathrm{E}\{J(\tau_i)\}$, $\chi_2 = \mathrm{E}\{J(\tau_i) - J(\tau_i - 1)\}/\mathrm{E}\{J(\tau_i)\}$, $\chi_3 = \mathrm{E}\{J(\tau_i) - J(\tau_i + P)\}/\mathrm{E}\{J(\tau_i)\}$ and $\chi_4 = \mathrm{E}\{J(\tau_i) - J(\tau_i - P)\}/\mathrm{E}\{J(\tau_i)\}$. We readily obtain

$$\chi_1 = \mathrm{E}\left\{|h_i(0)|^2\right\};\ \chi_2 = \mathrm{E}\left\{|h_i(L-1)|^2\right\}$$
$$\chi_3 = \chi_4 = 1 - \left(\frac{\sin(\pi V n/Q)}{V \sin(\pi n/Q)}\right)^2 \tag{23}$$

Since χ_1 and χ_2 are independent of V, the optimization problem (22) can be further simplified as

$$V^o \approx \arg\max_V \chi_3 \tag{24}$$

Fig. 6 shows a numerical example of the impact of tile size on $\{\chi_n\}_{n=1}^3$ when $N = 512$, $L = 16$ and $M = 2$ and $Q = 2^{\lfloor \log_2 MV \rfloor + 1}$. The exponential power delay profile introduced previously was considered. For this numerical example, it can be deduced that:

1) for the evaluated tile sizes, $V = 7$ will provide the best timing estimation performance;
2) since the timing offset error is dominated by the larger Pr_i, the estimation performance versus tile size V will encounter a floor due to the fact that χ_1 and χ_2 remain constant when varying V; further, $V = 3$ will yield performance close to those of $V = 5, 6, 7$;
3) the results hold true in the presence of CFOs.

The above results will be verified through simulations in Section V. For different signal parameters, the values for the best tile sizes may differ from those given above. These can be accurately predicted by eq. (24).

C. CFO estimation performance analysis

To analyze the performance of the proposed CFO estimator, we assume perfect timing, and use the Cramér-Rao bound associated with the estimation of the $\theta_{i,v}$'s based on the signal model in eq. (10), where the $\tilde{r}^{i,v}(n)$'s are treated as deterministic unknowns,[1] and then deduce bounds on the estimation of the ω_i's using the relationships in eq. (14). The obtained bound will be referred to the subspace decomposition based CRB (SD-CRB) since eq. (10) allows CFO estimation using subspace-based methods.

The SD-CRB of $\boldsymbol{\theta}$ is obtained along the same lines as in [24] and is found to be

$$\text{SD-CRB}_{(V,P)}(\boldsymbol{\theta}) = \frac{\sigma_v^2}{2}\left\{\sum_{p=0}^{P-1} \mathrm{Re}\Big\{\mathbf{D}_p^H \mathbf{T}^H \left(\mathbf{I} - \mathbf{G}\left(\mathbf{G}^H\mathbf{G}\right)^{-1}\mathbf{G}^H\right)\mathbf{T}\mathbf{D}_p\Big\}\right\}^{-1} \tag{25}$$

where $\boldsymbol{\theta} = [\boldsymbol{\theta}_1^T, \cdots, \boldsymbol{\theta}_M^T]^T$, $\boldsymbol{\theta}_i = [\theta_{i,0}, \cdots, \theta_{i,V-1}]^T$, $\mathbf{T} = [\frac{\partial(\boldsymbol{G}_0)}{\partial\theta_{1,0}}, \frac{\partial(\boldsymbol{G}_1)}{\partial\theta_{1,1}}, \cdots, \frac{\partial(\boldsymbol{G}_{MV})}{\partial\theta_{M,V-1}}]$, $\boldsymbol{G}_l$ is the lth column of matrix $\mathbf{G}$; and $\mathbf{D}_p = \mathrm{diag}\{\tilde{\boldsymbol{r}}_p\}$. Recall eq. (14), we have

$$\omega_i = \frac{N}{2\pi V}\boldsymbol{\zeta}^T\boldsymbol{\theta}_i - c_i$$

where $\boldsymbol{\zeta} = [1, \cdots, 1]^T$ and $c_i = i - 1 + \frac{1}{V}\sum_{v=0}^{V-1} v$. The SD-CRB for $\hat{\omega}_i$ can be expressed as

$$\text{SD-CRB}(\omega_i) = \left(\frac{N}{2\pi V}\right)^2 \boldsymbol{\zeta}^T \text{SD-CRB}_{(V,P)}(\boldsymbol{\theta}_i)\boldsymbol{\zeta} \tag{26}$$

where $\text{SD-CRB}_{(V,P)}(\boldsymbol{\theta}_i)$ is a sub-matrix of $\text{SD-CRB}_{(V,P)}(\boldsymbol{\theta})$. We can see later that the performance of the EFCE method with the proposed WSCTE estimator could approach the SD-CRB by selecting the title size V properly. It can be shown that $V = 1$ is optimal for CFO estimation in the absence of timing offset. When timing is required to be estimated, $V = 1$ will be shown in the simulation section to yield poor CFO estimation performance.

V. Simulation Results

A. Simulation setup

Consider a cooperative system with two relay nodes, i.e. $M = 2$. The total number of subcarriers of each OFDM block is $N = 512$. The training sequences of the relay nodes are uncorrelated and have the same power σ_{ts}^2. The CP and PP of the training sequences are selected to have lengths equal to 64 and 48, respectively. In order to satisfy the condition that $\max\{|\tau_i - \tau_j|\} < \min\{N_{dl}, N_{pp}\}$, we assume that the signal of relay node R_1 arrives at the destination node first in our simulation setup, and the differential propagation delay $\tau_2 - \tau_1$ is uniformly distributed within the interval $[0, 48]$. The tile subchannels allocated to the two relay nodes during the training period are distinct. To make sure Q is larger than MV, we select $Q = 2^{\lfloor \log_2 MV \rfloor + 1}$, where $\lfloor a \rfloor$ rounds a to the nearest integer smaller than or equal to a. Hence, the number

[1]Such an approach was adopted in [19] for the case of single CFO estimation

of null subcarriers is 256, 256, 128, 256, 192, 128, 64, and 256 when V increases from 1 to 8, respectively.

In the simulation, we assume that the CIR length is $L = 16$, and the channel taps $h_i(l)$ are uncorrelated zero-mean Gaussian random variables with exponential power delay profile $\mathrm{E}\left\{|h_i(l)|^2\right\}_{l=0}^{L-1} = C\exp(-0.2l)$, where C is a scalar factor that ensures that the total energy of the channel taps is normalized to unity. Correspondingly, the SNR of each relay node is equal to $\sigma_{ts}^2/(N\sigma_v^2)$. The channels for different nodes are assumed uncorrelated.

To quantify the degradation of the BER due to the residual timing and CFO, which are equal to the difference between the offset estimates fed back by the destination node and the actual offsets, information-bearing blocks are transmitted using a cooperative Alamouti space-time encoding and maximum likelihood detection assuming a perfect channel state information is performed.

B. Simulation results

In this section, we compare the estimation performance of the proposed algorithms and the conventional SAGE algorithm in [11] and TDM based S&C algorithm [15]. The SAGE estimation results shown are obtained at the 5th iteration and CIR are assumed to be known perfectly in each iteration. The length of TDM based training sequences is set to N/M to make a fair comparison. We also assume that there is no collision for TDM based synchronization.

Fig. 7 and Fig. 8 show the timing estimation performance of the proposed WSCTE with different tile sizes. The estimation performance is measured in terms of averaged (over the channel and relay nodes) standard deviation (STD) of the timing errors. As predicted in the previous section, we see that the WSCTE with tile size $V = 3, 5, 6, 7$ outperforms other selections significantly. Moreover, we can find that improvement shrinks for large tile sizes. The tile size $V = 3$ seems to provide sufficient accuracy. It can also be seen that WSCTE performance is dominated by multinode interference since it is not very sensitive to SNR. It can also be seen that the proposed WSCTE with tile size $V = 3$ outperforms TDM based and SAGE algorithms significantly.

Figures 9-11 compare the CFO estimation performance of EFCE with different tile sizes. The performance is measured in terms of averaged (over the channel and relay nodes) MSE. We set the frequency offsets to $\omega_1 = 0.35$ and $\omega_2 = 0.25$. It can be seen that EFCE with tile size $V = 1$ provides the best performance at low SNR. However, it exhibits an error floor at intermediate and high SNRs due to the residual timing errors. As shown in Fig. 9 and Fig. 10, we also notice that the performance of EFCE with the tile size that provides the best timing estimate, i.e. $V = 3$ in the above figures, achieves the SD-CRB. Moreover, we can see from Fig. 11 that the proposed EFCE, with tile size $V = 3$, outperforms the TDM based and SAGE algorithms.

The BER performance of an uncoded QPSK system is shown in Fig. 12. A cooperative Alamouti space-time encoding scheme is adopted and the channels, which take into account timing errors, are assumed to be known. The length of the

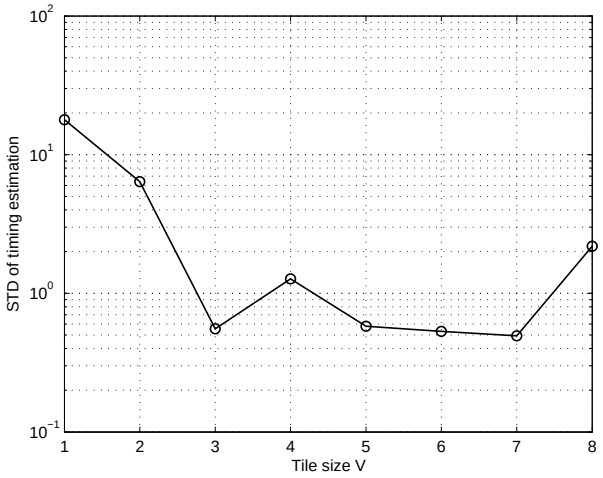

Fig. 7. WSCTE estimation performance versus tile size V, SNR=20dB

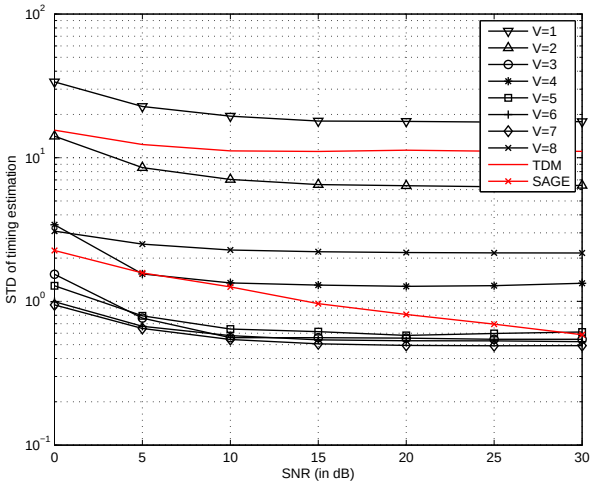

Fig. 8. Timing estimation performance versus SNR

CP for the data blocks is set to 20. As expected, SAGE and TDM-based algorithms are outperformed by the proposed algorithms. It can be seen that tile size $V = 3$ outperforms the other evaluated tile sizes at intermediate and high SNRs, and the corresponding BER performance is close to the ideal case scenario (no synchronization errors).

C. Optimal tile size selection for BER

As shown in WSCTE performance evaluation, larger tile sizes will provide better timing estimation performance. However, EFCE performance will decrease with increasing tile size. Due to the estimation floor of WSCTE, as discussed previously, we can conclude that a good BER performance is achieved by the smallest tile size with close-best timing performance. The optimal tile size can be predicted as shown in Section IV.B.

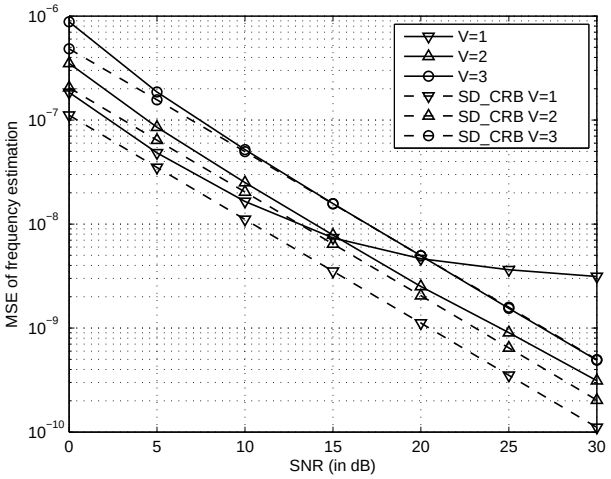

Fig. 9. EFCE estimation performance versus SNR

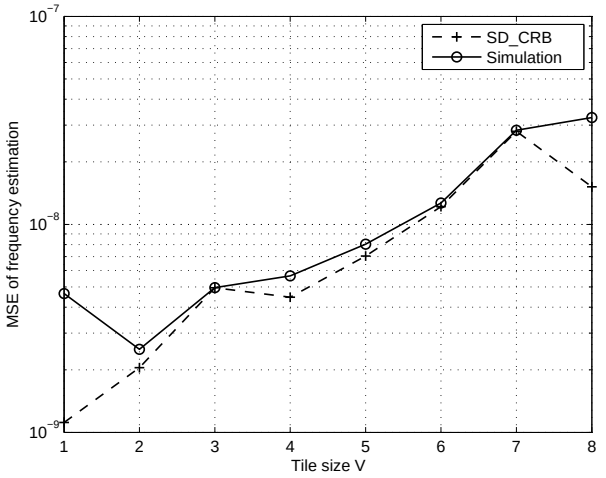

Fig. 10. EFCE estimation performance versus tile size V, SNR=20dB

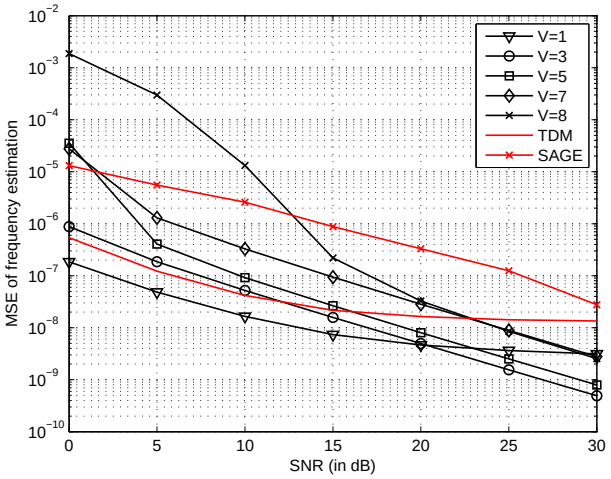

Fig. 11. CFO estimation performance versus SNR

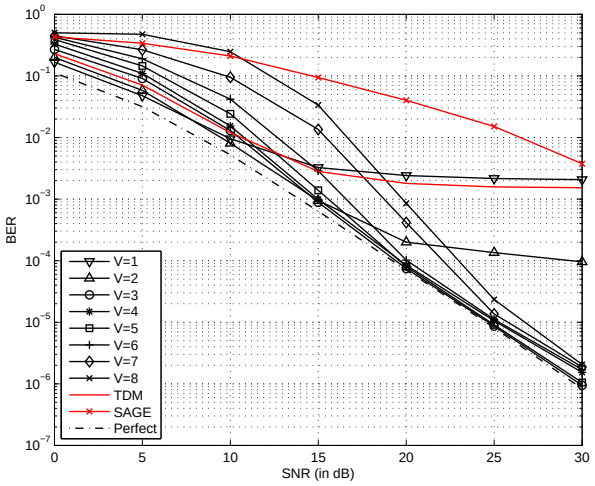

Fig. 12. BER performance versus SNR for uncoded QPSK

D. Computational Complexity

We briefly compare the complexities of the proposed synchronization algorithms and SAGE. Considering the number of complex multiplications as a complexity metric, the inversion of an $n \times n$ matrix requires $\mathcal{O}(n^3)$ operations, the SVD of $n \times n$ matrix requires $\mathcal{O}(n^3)$ operations, and the product of an $m \times r$ matrix with an $r \times n$ matrix requires $\mathcal{O}(mrn)$ operations.

Assume that the WSCTE and SAGE algorithms need to search over the same time interval of length, say K_t, for timing estimation. The complexity of WSCTE is $\mathcal{O}(K_t MN)$, and SAGE needs $\mathcal{O}(K_t MNLK_{it})$ operations, where K_{it} denotes the number of iterations. Regarding CFO estimation, SAGE takes $\mathcal{O}(MNLK_{it}K_f)$ operations, where $K_f > 10^3$ denotes the number of evaluated CFO offsets in each iteration. Compared to the complicated SAGE algorithm, the proposed EFCE only requires $\mathcal{O}(Q^3 + NQ)$ operations.

VI. Conclusion

We have addressed the problem of timing and frequency synchronization in OFDM-based cooperative systems. To avoid multi-parameter and multi-dimensional search required by the exact ML estimator, we divided the subcarriers of the pilot OFDM block into tile subchannels and performed a correlation-type algorithm for timing synchronization and an ESPRIT-type algorithm, exploiting null subcarriers, for frequency synchronization. By judiciously choosing the tile size, it was shown that the proposed algorithms outperform the existing TDM based algorithm and SAGE algorithm significantly. The proposed algorithms are also computationally much more attractive than SAGE.

Appendix A
Derivation of Equation (19-21)

We assume that subcarriers in a training sequence are uncorrelated and have the same power. Mathematically, this

$$\mathrm{E}\left\{J(\tau_i)-J(\tau_i+n)\right\}=\sum_{l=0}^{L-1}\alpha_l\Big(\mathrm{E}\left\{B(\tau_i+l)\right\}-\mathrm{E}\left\{B(\tau_i+l+n)\right\}\Big) \quad (39)$$

$$\mathrm{Var}\{J(\tau_i)-J(\tau_i+1)\}=\alpha_0^2\mathrm{Var}\{B(\tau_i)\}+\sum_{l=0}^{L-2}(\alpha_{l+1}-\alpha_l)^2\mathrm{Var}\{B(\tau_i+l+1)\}+\alpha_{L-1}^2\mathrm{Var}\{B(\tau_i+L)\} \quad (40)$$

$$\mathrm{Var}\{J(\tau_i)-J(\tau_i-1)\}=\alpha_0^2\mathrm{Var}\{B(\tau_i-1)\}+\sum_{l=0}^{L-2}(\alpha_l-\alpha_{l+1})^2\mathrm{Var}\{B(\tau_i+l)\}+\alpha_{L-1}^2\mathrm{Var}\{B(\tau_i+L-1)\} \quad (41)$$

$$\mathrm{Var}\{J(\tau_i)-J(\tau_i+nP)\}=\sum_{l=0}^{L-1}\alpha_l^2\Big(\mathrm{Var}\{B(\tau_i+l)\}+2\mathrm{E}\left\{B(\tau_i+l)\right\}\mathrm{E}\left\{B(\tau_i+l+nP)\right\}+\mathrm{Var}\{B(\tau_i+l+nP)\}-2\mathrm{E}\left\{B(\tau_i+l)B(\tau_i+l+np)\right\}\Big) \quad (42)$$

where

$$\mathrm{E}\left\{B(\tau_i+l)B(\tau_i+l+np)\right\}=2\xi(l+nP)\xi(l)\frac{\sigma_{ts}^8}{V^4}\mathrm{E}\left\{|h_i(l)|^2\right\}^2+\left(\xi(l)+\xi(l+nP)\right)\frac{\sigma_{ts}^6}{V^2}\mathrm{E}\left\{|h_i(l)|^2\right\}\sigma_v^2+\sigma_{ts}^4\sigma_v^4$$

assumption implies that

$$\mathrm{E}\left\{X_m(k_1)X_m^*(k_2)\right\} = \frac{\sigma_{ts}^2}{VP}\delta_{k_1-k_2} \quad (27)$$

$$\mathrm{E}\left\{X_m(k_1)X_m(k_2)\right\} = 0 \quad (28)$$

where E is the statistical expectation operator and $\delta_{k_1-k_2}$ is the Kronecker delta. Since we assume that the noise is an AWGN with variance σ_v^2, we have that

$$\mathrm{E}\left\{\upsilon(n_1)\upsilon^*(n_2)\right\} = \sigma_v^2\delta_{n_1-n_2} \quad (29)$$

$$\mathrm{E}\left\{\upsilon(n_1)\upsilon(n_2)\right\} = 0 \quad (30)$$

Using eq. (27-30) and $P > L$, we readily obtain

$$\mathrm{E}\left\{|d_i(\tilde{\tau}_i+l)|^2\right\}=\sigma_{ts}^2\sigma_v^2 \quad (31)$$

$$\mathrm{E}\left\{|d_i(\tilde{\tau}_i+l)|^4\right\}=2\sigma_{ts}^4N\sigma_v^4 \quad (32)$$

$$\mathrm{E}\left\{|Z_{i,i}(\tilde{\tau}_i+l,0)|^2\right\}=\xi(\varrho_l)\frac{\sigma_{ts}^4}{V^2}\mathrm{E}\left\{|h_i(\bar{\varrho}_l)|^2\right\} \quad (33)$$

$$\mathrm{E}\left\{|Z_{i,i}(\tilde{\tau}_i+l,0)|^4\right\}=2\xi^2(\varrho_l)\frac{\sigma_{ts}^8}{V^4}\mathrm{E}\left\{|h_i(\bar{\varrho}_l)|^2\right\}^2 \quad (34)$$

where $\varrho_l=\tilde{\tau}_i+l-\tau_i$, $\bar{\varrho}_l=\mathrm{mod}(\varrho_l,P)$ and

$$\xi(\varrho_l)=\begin{cases}V^2 & 0\le\varrho_l<P;\\ \left(\frac{\sin(\pi Vn/Q)}{\sin(\pi n/Q)}\right)^2 & nP\le\varrho_l<(n+1)P;\end{cases} \quad (35)$$

$$\mathrm{E}\left\{|h_i(\bar{\varrho}_l)|^2\right\}=\sum_{k=0}^{L-1}\sigma_{h_i(k)}^2\delta_{k-\bar{\varrho}_l} \quad (36)$$

where $\sigma_{h_i(k)}^2$ is the power distribution of the kth channel tap of the ith relay. Following eq. (31-34), we have that

$$\mathrm{E}\left\{B(\tilde{\tau}_i+l)\right\}=\xi(\varrho_l)\frac{\sigma_{ts}^4}{V^2}\mathrm{E}\left\{|h_i(\bar{\varrho}_l)|^2\right\}+\sigma_{ts}^2\sigma_v^2 \quad (37)$$

$$\mathrm{Var}\{B(\tilde{\tau}_i+l)\}=\xi^2(\varrho_l)\frac{\sigma_{ts}^8}{V^4}\mathrm{E}\left\{|h_i(\bar{\varrho}_l)|^2\right\}^2+2\xi(\varrho_l)\frac{\sigma_{ts}^6}{V^2}\mathrm{E}\left\{|h_i(\bar{\varrho}_l)|^2\right\}\sigma_v^2+\sigma_{ts}^4N\sigma_v^4 \quad (38)$$

where $B(\tilde{\tau}_i+l)\triangleq|Z_{i,i}(\tilde{\tau}_i+l,0)+d_i(\tilde{\tau}_i+l)|^2$. Eq. (39-42) can thus be readily obtained.

References

[1] A. Sendonaris, E. Erkip, and B. Aazhang, "User cooperation diversity. Part I. System description," *IEEE Trans. Commun.*, vol. 51, no. 11, pp. 1927–1938, Nov. 2003.

[2] J. Laneman and G. Wornell, "Distributed space-time-coded protocols for exploiting cooperative diversity in wireless networks," *IEEE Trans. Inf. Theory*, vol. 49, no. 10, pp. 2415–2425, Oct. 2003.

[3] S. Jagannathan, H. Aghajan, and A. Goldsmith, "The effect of time synchronization errors on the performance of cooperative MISO systems," in *Proc. IEEE Global Telecommunications Conference Workshops GlobeCom Workshops 2004*, 29 Nov.-3 Dec. 2004, pp. 102–107.

[4] Y. Mei, Y. Hua, A. Swami, and B. Daneshrad, "Combating synchronization errors in cooperative relays," in *Proc. IEEE International Conference on Acoustics, Speech, and Signal Processing*, vol. 3, 18-23 Mar. 2005, pp. 369–372.

[5] Z. Li and X. Xia, "A Simple Alamouti Space-Time Transmission Scheme for Asynchronous Cooperative Systems," *Signal Processing Letters, IEEE*, vol. 14, no. 11, pp. 804–807, Nov. 2007.

[6] F. Ng and X. Li, "Cooperative STBC-OFDM Transmissions with Imperfect Synchronization in Time and Frequency," in *Conference Record of the Thirty-Ninth Asilomar Conference on Signals, Systems and Computers*, 28 Oct.-1 Nov. 2005, pp. 524–528.

[7] M.-K. Oh, X. Ma, G. Giannakis, and D.-J. Park, "Cooperative synchronization and channel estimation in wireless sensor networks," in *Conference Record of the Thirty-Seventh Asilomar Conference on Signals, Systems and Computers*, vol. 1, 9-12 Nov. 2003, pp. 238–242.

[8] J.-J. van de Beek, P. Borjesson, M.-L. Boucheret, D. Landstrom, J. Arenas, P. Odling, C. Ostberg, M. Wahlqvist, and S. Wilson, "A time and frequency synchronization scheme for multiuser OFDM," *IEEE J. Sel. Areas Commun.*, vol. 17, no. 11, pp. 1900–1914, Nov. 1999.

[9] M. Morelli, "Timing and frequency synchronization for the uplink of an OFDMA system," *IEEE Trans. Commun.*, vol. 52, no. 2, pp. 296–306, Feb. 2004.

[10] M.-O. Pun, M. Morelli, and C.-C. Kuo, "Maximum-likelihood synchronization and channel estimation for OFDMA uplink transmissions," *IEEE Trans. Commun.*, vol. 54, no. 4, pp. 726–736, Apr. 2006.

[11] J.-H. Lee and S.-C. Kim, "Time and Frequency Synchronization for OFDMA Uplink System using the SAGE Algorithm," *IEEE Trans. Wireless Commun.*, vol. 6, no. 4, pp. 1176–1181, Apr. 2007.

[12] A. Saemi, J.-P. Cances, and V. Meghdadi, "Synchronization algorithms for MIMO OFDMA systems," *IEEE Trans. Wireless Commun.*, vol. 6, no. 12, pp. 4441–4451, Dec. 2007.

[13] Z. Cao, U. Tureli, and Y. Yao, "Deterministic multiuser carrier-frequency offset estimation for interleaved OFDMA uplink," *IEEE Trans. Commun.*, vol. 52, no. 9, pp. 1585–1594, Sep. 2004.

[14] J. Lee, S. Lee, K.-J. Bang, S. Cha, and D. Hong, "Carrier Frequency Offset Estimation Using ESPRIT for Interleaved OFDMA Uplink Systems," *IEEE Trans. Veh. Technol.*, vol. 56, no. 5, pp. 3227–3231, Sep. 2007.

[15] T. Schmidl and D. Cox, "Robust frequency and timing synchronization for OFDM," *IEEE Trans. Commun.*, vol. 45, no. 12, pp. 1613–1621, Dec. 1997.

[16] H. Minn, V. Bhargava, and K. Letaief, "A robust timing and frequency synchronization for OFDM systems," *IEEE Trans. Wireless Commun.*, vol. 2, no. 4, pp. 822–839, Jul. 2003.

[17] M. Ghogho and A. Swami, "Frame and Frequency Acquisition for OFDM," *Signal Processing Letters, IEEE*, vol. 15, pp. 605–608, 2008.

[18] M. Morelli and U. Mengali, "An improved frequency offset estimator for OFDM applications," *Communications Letters, IEEE*, vol. 3, no. 3, pp. 75–77, Mar. 1999.

[19] M. Ghogho, P. Ciblat, A. Swami, and P. Bianchi, "Training Design for Repetitive-Slot-based CFO estimation in OFDM," *IEEE Trans. Signal Process.*, vol. xx, no. xx, pp. xxx–xxx, Forthcoming 2009.

[20] M. Ghogho, A. Swami, and G. Giannakis, "Optimized null-subcarrier selection for CFO estimation in OFDM over frequency-selective fading channels," in *Proc. IEEE Global Telecommunications Conference*, vol. 1, 25-29 Nov. 2001, pp. 202–206.

[21] R. Bachl, "The forward-backward averaging technique applied to TLS-ESPRIT processing," *IEEE Trans. Signal Process.*, vol. 43, no. 11, pp. 2691–2699, Nov. 1995.

[22] X. Y. Fu and H. Minn, "Initial uplink synchronization and power control (ranging process) for OFDMA systems," in *Proc. IEEE Global Telecommunications Conference*, vol. 6, 29 Nov.-3 Dec. 2004, pp. 3999–4003.

[23] E. Zhou, H. Zhao, and W. B. Wang, "Timing Synchronization for Interleaved OFDMA Uplink System," in *Proc. International Conference on Communications, Circuits and Systems*, vol. 2, 25-28 Jun. 2006, pp. 1147–1152.

[24] P. Stoica and N. Arye, "MUSIC, maximum likelihood, and Cramer-Rao bound," *Acoustics, Speech, and Signal Processing [see also IEEE Transactions on Signal Processing], IEEE Transactions on*, vol. 37, no. 5, pp. 720–741, May 1989.